Argonaute-independent, Dicer-dependent antiviral defense against RNA viruses

Yukiyo Sato [a, *], Hideki Kondo [a], and Nobuhiro Suzuki [a, 1]

[a] Institute of Plant Science and Resources, Okayama University, Kurashiki, Okayama 710-0046, Japan

[1] To whom correspondence may be addressed. Corresponding Author: Dr. Nobuhiro Suzuki
ORCID ID, http://orcid.org/0000-0003-0097-9856
Agrivirology Laboratory
Institute of Plant Science and Resources
Okayama University
Kurashiki, Okayama 710-0046, Japan
Tel. 81(86) 434-1230
Fax. 81(86) 434-1232
e-mail. nsuzuki@okayama-u.ac.jp

*Present Address: Institute for Plant Sciences, University of Cologne, Cologne, Germany

Short title: AGO-independent, Dicer-independent antiviral defense

Summary (190 words)

Antiviral RNA interference (RNAi) is conserved from yeasts to mammals. Dicer recognizes and cleaves virus-derived double-stranded RNA (dsRNA) and/or structured single-stranded RNA (ssRNA) into small interfering RNAs (siRNAs), which guide effector Argonaute to homologous viral RNAs for digestion and inhibit virus replication. Thus, Argonaute is believed to be essential for antiviral RNAi. Here, we show Argonaute-independent, Dicer-dependent antiviral defense against dsRNA viruses using *Cryphonectria parasitica* (chestnut blight fungus), which is a model filamentous ascomycetous fungus and hosts a variety of viruses. The fungus has two dicer-like genes (*dcl1* and *dcl2*) and four argonaute-like genes (*agl1* to *agl4*). We prepared a suite of single to quadruple *agl* knockout mutants with or without *dcl* disruption. We tested these mutants for antiviral activities against diverse dsRNA viruses and ssRNA viruses. Although both DCL2 and AGL2 worked as antiviral players against some RNA viruses, DCL2 without argonaute was sufficient to block the replication of other RNA viruses. Overall, these results indicate the existence of a Dicer-alone defense and different degrees of susceptibility to it among RNA viruses. We discuss what determines the great difference in susceptibility to the Dicer-only defense.

Keywords: RNAi, RNA silencing, Argonaute, Dicer, RNA virus, fungal virus, chestnut blight

Significance (<120 words)

RNA interference is the primary antiviral defense in plants, fungi, and invertebrates, wherein Dicer cleaves viral dsRNA into siRNAs, while Argonaute as the effector digests target viral RNA using virus-derived guide siRNAs. However, an interesting question remains unanswered; Does Dicer alone play an antiviral role in the absence of Argonaute? This question is difficult to answer because disruption of all members of the Argonaute family would lead to lethality. Herewith we addressed this long-standing question by preparing a suite of single and multiple Dicer and Argonaute mutants of a model filamentous host fungus, *Cryphonectria parasitica*. We demonstrated Dicer-alone defense—the dispensability of Argonaute in antiviral defense—against some RNA viruses, while Argonaute is required for full-scale antiviral defense against others.

Antiviral RNA silencing or RNA interference (RNAi) is a small RNA–mediated defense mechanism that has been conserved from unicellular yeasts to multicellular mammals (1-4). Viral double-stranded RNAs (dsRNAs) or structured single-stranded RNAs (ssRNAs) are sensed and digested by the dsRNA-specific ribonuclease Dicer into small-interfering RNAs (siRNAs), which then serve as a guide and enhance the degradation and translational repression of target viral RNAs by the effector ribonuclease Argonaute (5, 6). In plants and nematodes, host-encoded RNA-dependent RNA polymerase (RDR) is involved in the amplification cycle of siRNA production (5, 7). Therefore, deficiency of these key genes in the RNAi antiviral pathway results in enhanced virus replication and symptom induction (8-11). One of the important unanswered questions about antiviral RNAi is whether Dicer activity without Argonaute effectors is functional in antiviral defense. Although this issue has been discussed previously (12), no conclusions have been drawn. This question can be tested only by disrupting all Argonaute genes in an organism. In plants and animals, however, multiple knockouts of all Argonaute genes could be difficult because of the great numbers of paralogous Argonaute genes, several of which are involved in the microRNA (miRNA) pathway crucial for development (13, 14). For example, the model plant *Arabidopsis thaliana* has ten (15), human has eight (16), the model fly *Drosophila melanogaster* has five (17), and the model nematode *Caenorhabditis elegans* has 27 Argonaute paralogs (18), which show pleiotropic roles.

The chestnut blight fungus, *Cryphonectria parasitica*, is a destructive plant pathogen as well as a filamentous model fungus for studying virus–virus and virus–host interactions (19, 20). This ascomycetous fungus has two dicer-like (*dcl1* and *dcl2*), four argonaute-like (*agl1* to *agl4*), and four *rdr* (*rdr1* to *rdr4*) genes (10, 21, 22). By utilizing the prototype ssRNA monopartite hypovirus Cryphonectria hypovirus 1 (CHV1) with a capsidless nature, researchers have shown that *dcl2* and *agl2* are required for antiviral RNAi (10, 21). Unlike in plants, no *rdr* gene in *C. parasitica* is involved in antiviral RNAi, indicating that no amplification step of siRNA is required for it (22); instead, transcription of the key genes *dcl2* and *agl2* is markedly induced upon virus infection (21, 23). The mechanisms governing these regulations are largely unknown. Another unique feature of *C. parasitica* is that DCL2 plays a dual role transcriptionally and post-transcriptionally. As observed in other organisms, DCL2 functions as one of the key RNAi genes to dice viral dsRNAs (10, 24). In addition, DCL2 serves as a positive feedback player to transcriptionally induce many host genes, including *dcl2* and *agl2*, an action that requires the general transcriptional co-activator SAGA (*S*pt-*A*da-*G*cn5 *a*cetyltransferase) complex (25, 26). This transcriptional regulation can be suppressed by a viral RNA silencing suppressor (RSS), such as CHV1 p29, via an unknown mechanism (21, 25, 27). Some of the upregulated host genes alleviate virus symptoms without affecting virus replication,

leading researchers to propose an additional layer of host defense (symptom mitigation) (25). We have previously shown that the highly induced RNAi state, either by an infecting virus or transgenic expression of dsRNA, can eliminate a preexisting heterologous dsRNA virus, Rosellinia necatrix victorivirus 1 (RnVV1) with an undivided, encapsidated dsRNA genome (23). Surprisingly, *dcl2* but not *agl2* is required for elimination or clearance of this virus. There are two possibilities to explain this phenomenon: (1) *agl* genes other than *agl2* function as an effector of antiviral RNAi and (2) DCL2 is sufficient for virus interference.

In the current study, we show Dicer-dependent, Argonaute-independent RNAi in *C. parasitica* against multiple RNA viruses such as RnVV1, and the different levels of susceptibility to this Dicer-only antiviral defense among RNA viruses. We made this discovery by preparing a suite of deletion mutants lacking single or multiple *agl* genes with or without *dcl* disruption.

Results

Establishment and phenotypes of *dcl*/*agl* single and multiple knockout *C. parasitica* strains.

Although the function of *C. parasitica agl1*, *agl3*, and *agl4* remains unknown, all of them, in addition to *agl2*, encode typical Argonaute domains (28) (Fig. 1*A*). We first prepared single and multiple *agl* disruptants, including a triple *agl* mutant (Δ*agl1/3/4*) and a quadruple *agl* mutant (Δ*aglQ*), in *C. parasitica* strain DK80 with or without the other key RNAi gene *dcl2* disrupted (see Table 1 for names and genotypes of all the mutants). Strain DK80 is an EP155 (a wild-type strain) mutant that lacks a *ku80* ortholog (*cpku80*, required for non-homologous end-joining DNA repair) to increase homologous recombination (HR) efficiency (29). We replaced the coding sequence of *dcl*/*agl* genes with selectable marker genes (SMGs, antibiotic resistance genes) by HR (*SI Appendix*, Fig. S1). For multiple gene disruption, we utilized three SMGs and a Cre-*loxP*-mediated marker recycling system, in which Cre recombinase catalyzed *loxP* site-specific recombination to remove SMGs (30) (*SI Appendix*, Fig. S2). In all the generated mutants, we validated precise target disruption by polymerase chain reaction (PCR) and Southern blotting (Fig. 1*B* and *SI Appendix*, Fig. S3). Importantly, all the *dcl*/*agl* disruptants manifested a normal growth phenotype on potato dextrose agar plates, similarly to the original strain DK80 (*SI Appendix*, Fig. S4).

DCL2 but not any single AGL efficiently restricts RnVV1.

First, we analyzed RnVV1 accumulation, together with CHV1 accumulation in parallel, in the single *dcl*/*agl* knockout DK80 mutant series, namely Δ*dcl1*, Δ*dcl2*, Δ*agl1*, Δ*agl2*, Δ*agl3*, and Δ*agl4* (Table 1, Fig. 2). These mutants, DK80, and EP155 were each co-cultured with respective virus donor fungal

strains (Table 1, Fig. 2*A*). We detected viral RNA in the virus-free or virus-infected recipients by northern hybridization using virus-specific complementary DNA (cDNA) probes against regions inside part encoding viral RNA-dependent RNA polymerase (RdRP) (*SI Appendix*, Table S2). The northern hybridization showed clear RnVV1 signal only in Δ*dcl2* and none in EP155, DK80, Δ*dcl1*, Δ*agl1*, Δ*agl2*, Δ*agl3*, or Δ*agl4*, after RnVV1-infection (Fig. 2*B*). Compared with EP155 and DK80, CHV1 accumulation was clearly increased in Δ*dcl2* and Δ*agl2*, but not in Δ*dcl1*, Δ*agl1*, Δ*agl3*, or Δ*agl4* (Fig. 2*C*). These CHV1 results are consistent with the previous results with the EP155 genetic background (10, 21). Recipient strains have been reported to carry over a minor portion of a donor's karyons (31). To eliminate the possibility of heterokaryon effects on RnVV1 accumulation, we next transfected DK80, Δ*dcl2*, and Δ*agl2* with purified RnVV1 virions (Fig. 2*D*). Semi-quantitative reverse transcription (semi-qRT)-PCR using a constant amount of substrate RNA showed that RnVV1 was accumulated comparably in DK80 and Δ*agl2*, while there was more in Δ*dcl2* transfectants (Fig. 2*E*). Northern hybridization also showed clear RnVV1 signal only in Δ*dcl2*, and none in DK80 or Δ*agl2* in the transfectants (Fig. 2*E*).

Taken together, these results indicate that *dcl2* alone is responsible for RnVV1 reduction, while disruption of *dcl1*, *agl1*, *agl2*, *agl3*, or *agl4* did not allow enhanced RnVV1 replication, suggesting that *agl* genes function redundantly or no *agl* genes are involved in the anti-RnVV1 response in *C. parasitica*. By contrast, both *dcl2* and *agl2* are required for CHV1 repression, as reported previously with the *C. parasitica* EP155 genetic background (10, 21).

A *C. parasitica* reovirus MyRV2 is also strongly silenced by *dcl2* but not by *agl2*

Researchers initially assumed that the susceptibility of RnVV1 to the Dicer-alone defense was associated with its poor adaptability to the host fungus *C. parasitica*, a non-native host of RnVV1. RnVV1 is from another ascomycetous phytopathogen, *Rosellinia necatrix* (31). Thus, we screened a collection of viruses, which were originally isolated from *C. parasitica*, for those with RnVV1-like behaviors, namely restricted by *dcl2*, but not *agl2* (*SI Appendix*, Fig. S5). The tested *C. parasitica* viruses include three hypoviruses (a capsidless monopartite ssRNA genome) and two mycoreoviruses (a multi-segmented, monoparticulate dsRNA genome), namely Cryphonectria hypovirus 2 (CHV2), Cryphonectria hypovirus 3 (CHV3), Cryphonectria hypovirus 4 (CHV4), mycoreovirus 1 (MyRV1), and mycoreovirus 2 (MyRV2) (Table 1 and *SI Appendix*, Table S3). We used these viruses to inoculate DK80 and its single and multiple mutants Δ*dcl2*, Δ*agl2*, and Δ*dcl2*Δ*agl2* via hyphal fusion (Fig. 2*A*). We detected viral RNA in the recipient strains before and after the infection by using northern hybridization with probes targeting viral RdRP-encoding segments (*SI Appendix*, Table S2). CHV2, CHV3, CHV4, and MyRV1 obviously accumulated in DK80 and showed slight or no increase in Δ*dcl2*, Δ*agl2*, and a double mutant Δ*dcl2*Δ*agl2* (*SI Appendix*, Fig. S5*A*). In contrast, we did not detect MyRV2 in DK80 and Δ*agl2*, but it highly accumulated in Δ*dcl2* and Δ*dcl2*Δ*agl2*, similarly to RnVV1 (*SI*

Appendix, Fig. S5*B*). Thus, we subsequently investigated the possibility of Argonaute-independent antiviral silencing using RnVV1 and MyRV2.

Argonaute-independent, Dicer-dependent defense against RnVV1 and MyRV2

To test the possible functional redundancy of *agl* genes in the anti-RnVV1 and MyRV2 defense, we analyzed the antiviral ability of a subset of single to multiple *dcl2*/*agl* knockout *C. parasitica* strains and a *dcl2*-complemented strain for Δ*dcl2*Δ*aglQ* (Fig. 3). We inoculated each fungal strain with each virus alone via hyphal fusion (Fig. 2*A*). We electrophoresed total RNA (viral and host ssRNA and dsRNA) purified from virus-free and virus-infected strains, stained it with ethidium bromide (EtBr) (Fig. 3*A*–*E*, upper panel), and subjected it to northern hybridization with probes targeting a viral RdRP-encoding region (Fig. 3*A*–*E*, lower panel).

RnVV1 and MyRV2 were highly accumulated in the mutants lacking *dcl2* (Δ*dcl2*, Δ*dcl2*Δ*agl2*, and Δ*dcl2*Δ*aglQ*) at a level detectable by EtBr (less sensitive), which we confirmed by northern hybridization (more sensitive), but not in DK80 and the other mutants lacking only *agl* genes (Δ*agl2*, Δ*agl1/3/4*, and Δ*aglQ*) (Fig. 3*A* and *B*). DCL2-dependent, AGL-independent restriction of these two dsRNA viruses is supported by the observation that transgenic supply of *dcl2* restored the virus restriction phenotype in the Δ*dcl2*Δ*aglQ* background (Δ*dcl2*Δ*aglQ*+*dcl2*) (Figs. 3*A* and *B*). We also performed real-time qRT-PCR and semi-qRT-PCR in the same total RNA samples. We detected RnVV1 and MyRV2 in all the recipients after virus inoculation, but the signals were stronger in the mutants lacking *dcl2* than in DK80 and the other mutants, which was more obvious for MyRV2 than for RnVV1 (over two orders of magnitude for RnVV1 and four orders of magnitude for MyRV2) (*SI Appendix*, Fig. S6). The difference in semi-qRT-PCR signals between DK80 and the mutants lacking only *agl* genes was not associated with the presence or absence of particular *agl* genes (*SI Appendix*, Fig. S6*B*). We obtained similar results by qRT-PCR, northern hybridization and semi-qRT-PCR using ssRNA-enriched fraction (containing virus mRNAs) in independent experiments (*SI Appendix*, Fig. S7). Viral symptom observation also implied involvement or non-involvement of *dcl2* and *agl*, respectively, in the symptom alteration (Fig. 4 and *SI Appendix*, Fig. S8). In DK80 and the mutants lacking only *agl* (Δ*agl2*, Δ*agl1/3/4*, Δ*aglQ*, and Δ*dcl2*Δ*aglQ*+*dcl2*), RnVV1 and MyRV2 induced mild or no symptoms, respectively. RnVV1 and MyRV2 exhibited opposite symptom patterns in DK80. The RnVV1-induced symptoms were not obvious in the mutants lacking *dcl2* (Δ*dcl2*, Δ*dcl2*Δ*agl2*, and Δ*dcl2*Δ*aglQ*), while the other mutants showed a slight reduction in aerial hyphae, implying the involvement of *dcl2* in symptom induction by RnVV1. In contrast, MyRV2 reduced the growth rate in the mutants lacking *dcl2*, suggesting that *dcl2* is involved in the

196 mitigation of MyRV2-caused symptoms.

197 To examine viral impacts on transcriptome and the expression of RNAi genes, RNA-Seq analysis
198 was performed in virus-free and virus-infected DK80 and Δ*dcl2*. In the absence of virus, DK80 and
199 Δ*dcl2* showed similar transcriptomic profiles (Fig. 5*A*). RnVV1 induced relatively small changes in
200 the transcriptomes in DK80 and Δ*dcl2* (Fig. 5*A* and *B*). MyRV2 induced little change in the
201 transcriptome in DK80 but larger changes in the transcriptome of Δ*dcl2* (Fig. 5*A* and *B*), consistently
202 with the symptom severity (Fig. 4). In the absence of virus, the antiviral *dcl* and *agl* genes, namely
203 *dcl2* and *agl2*, were more expressed than the others, namely *dcl1*, *agl1*, *agl3*, and *agl4*, (Fig. 5*C*). In
204 DK80, RnVV1 upregulated *dcl2* and *agl2* as well as *rdr4*, but not the other RNAi-related genes (Fig.
205 5*C* and *D*). The expression of any of the RNAi-related genes remained unaltered upon inoculation
206 by MyRV2 (Fig. 5*D*), likely due to no or little accumulation of MyRV2 in the recipients (*SI Appendix*,
207 Fig. S6 and S7*B*).

208 These results collectively indicate that *C. parasitica dcl2* predominantly contributes to
209 RnVV1 and MyRV2 reduction and likely host symptom alteration, but no *agl* genes contribute to
210 it, even redundantly.

211

212 **Different *agl2* requirement patterns for antiviral responses against the other viruses**

213 To compare with RnVV1 and MyRV2, we also tested the antiviral ability of the same *C. parasitica*
214 mutants against MyRV1 (a close relative to MyRV2), CHV1 (a model ssRNA mycovirus), and CHV1-
215 Δp69 (a mutant of CHV1 lacking an RSS p29) (Fig. 3*C–G*). MyRV1 and CHV1 were highly
216 accumulated in the RNAi-competent DK80 based on EtBr staining of the agarose gel (Fig. 3*C–E*)—
217 considering the band intensity of the genomic dsRNA (multisegmented MyRV1) or replicative form
218 dsRNA of the genomic and defective (D1 and D2) (CHV1)—unlike RnVV1 and MyRV2 (Fig. 3*A* and
219 *B*). The difference in the accumulation level of MyRV1 among DK80 and the mutants was smaller,
220 compared to the dramatic difference of RnVV1 and MyRV2 accumulation in the presence or absence of
221 *dcl2* (Fig. 3*A-C* and *SI Appendix*, Fig. S6A). Full-length CHV1 and CHV1-Δp69 replicative form
222 dsRNA accumulated more in the mutants lacking *dcl2* and/or *agl2* compared with DK80 and Δ*agl1/3/4*
223 (Fig. 3*D-E* and *SI Appendix*, Figs. S6A and S7A). Defective interfering (DI) RNAs, which are produced
224 spontaneously via internal deletion, are associated with CHV1 infection. We observed two types of DI
225 RNAs (D1 and D2) in this study that were DCL2-depndent and -independent, respectively. The *dcl2*-
226 dependent CHV1 DI RNA (32) was increased in DK80 and Δ*agl1/3/4* to a comparable level ("D1" in
227 Fig. 3*D*), suggesting no contribution of *agl1*, *agl3*, and *agl4* to the production of this defective RNA.
228 CHV1 accumulated additional defective RNA in the mutants lacking *dcl2* and/or *agl2*, but not in DK80
229 and Δ*agl1/3/4* ("D2" in Fig. 3*D*). DCL2 appeared to contribute to lower CHV1-Δp69 in the absence

AGL2 (Fig. 3*E*). A similar trend was observed by qRT-PCR assay (*SI Appendix*, Figs. S6A and S7A). These results imply that full-scale anti-CHV1-Δp69 requires both AGL2 and DCL2, and DCL2 alone functions to reduce replicative dsRNA of CHV1-Δp69 to some extent. Upon infection by MyRV1 and CHV1-Δp69, DK80 and Δ*agl1/3/4* induced the expression of *dcl2* and *agl2* (Fig. 3*F* and *G*). These data suggest no contribution of *agl1*, *agl3*, or *agl4* to the regulation of *dcl2* and *agl2*, where SAGA and DCL2 play key roles (25, 26).

In DK80, MyRV1, CHV1, and CHV1-Δp69 induced strong symptoms which were unaltered in Δ*agl1/3/4*, suggesting *agl1*, *agl3*, or *agl4* have no effect on viral symptom expression (Fig. 4 and *SI Appendix*, Fig. S8). CHV1 and CHV1-Δp69 severely reduced colony growth in the mutants lacking *dcl2* and/or *agl2* (Δ*dcl2*, Δ*agl2*, Δ*dcl2*Δ*agl2*, Δ*aglQ*, Δ*dcl2*Δ*aglQ*, and Δ*dcl2*Δ*aglQ*+*dcl2*), suggesting contribution of both *dcl2* and *agl2* to symptom mitigation. MyRV1 induced slightly differential symptoms in the mutants lacking *dcl2* compared with DK80 and the other mutants, as observed previously in EP155 Δ*dcl2* (23), suggesting contribution of *dcl2* to the symptom alteration.

The virus-induced transcriptomic change was bigger in DK80 and Δ*dcl2* inoculated with MyRV1, CHV1, and CHV1-Δp69 compared with those inoculated with RnVV1 and MyRV2 (Fig. 5*A* and *B*), consistent with the higher level of viral accumulation and symptom induction (Fig. 4 and *SI Appendix*, Fig. S8). The degree of change in transcriptomic profiles between DK80 and Δ*dcl2* differs depending on viruses (Fig. 5*A*), while the number of genes differentially expressed by MyRV1, CHV1, and CHV1-Δp69 was comparable between DK80 and Δ*dcl2* (Fig. 5*B*). Inoculation of MyRV1 and CHV1-Δp69 as well as RnVV1 upregulated *dcl2*, *agl2* and as well as *rdr4*, but not the other RNAi-related genes (Fig. 5*C* and *D*). Inoculation of CHV1 did not significantly change the expression of any of the RNAi-related genes (Fig. 5*C* and *D*), which could be explained by the function of its p29 RSS (21, 25, 27).

Taken together, these results suggest that (1) *C. parasitica agl1*, *agl3*, and *agl4* are neither induced by the tested viruses nor involved in antiviral function against MyRV1, CHV1, and CHV1-Δp69; (2) *agl2* shows antiviral effects against the three viruses relatively highly accumulated in the RNAi-competent DK80; (3) *dcl2* contributes to viral reduction in both the presence and absence of an RSS p29 in CHV1 (CHV1-Δp69).

Small RNA analysis provides insights into the Dicer-alone anti-RnVV1 defense

We were interested in virus-derived small RNA (vsRNA) accumulation in the presence or absence of *agl* genes in *C. parasitica*, where the DCL2-dependent antiviral defense operated. To this end, we analyzed vsRNA profiles in DK80, Δ*dcl2*, Δ*agl2*, Δ*aglQ*, Δ*dcl2*Δ*aglQ*, and Δ*dcl2*Δ*aglQ*+*dcl2*, infected by each of RnVV1, MyRV2, MyRV1, and CHV1. In DK80, vsRNAs of RnVV1, MyRV1, and

CHV1 peaked at 20 or 21 nucleotides (nt) for either strand, while vsRNAs of MyRV2 were hardly detected (Fig. 6). In the mutants lacking *agl* genes but carrying *dcl2* gene (Δ*agl2*, Δ*aglQ*, and Δ*dcl2*Δ*aglQ*+*dcl2*), vsRNAs of RnVV1, MyRV1, and CHV1 retained a peak at 20 or 21 nt with changes in relative vsRNA abundance compared to those in DK80, while vsRNAs of MyRV2 were still hardly detected (Fig. 6). The poor detection of vsRNA reads of MyRV2 in the *dcl2*-carrying fungal strains is likely due to no or little accumulation of MyRV2 which is highly susceptible to the DCL2-dependent defense (*SI Appendix*, Figs. S6 and S7*B*). Surprisingly, even in the absence of Δ*dcl2*, positive- and negative-strand siRNAs derived from RnVV1 clearly peaked at 23 nt (Δ*dcl2*) or 22–23 nt (Δ*dcl2*Δ*aglQ*), a shift from the peak at 20–21 nt for DK80, Δ*agl2*, Δ*aglQ*, and Δ*dcl2*Δ*aglQ*+*dcl2* (Fig. 6). This size class of small RNAs may have been generated in a Dicer-independent way, as occurs in a filamentous fungus *Neurospora crassa* (33), or by DCL1. As reported earlier for the *C. parasitica* EP155 strain (25), the absence of *dcl2* (Δ*dcl2*, Δ*dcl2*Δ*aglQ*) resulted in high accumulation of vsRNAs corresponding to the positive strand of CHV1—with a lack of sharp peaks at 20 or 21 nucleotides (nt)—with no or little negative strand vsRNAs (Fig. 6). The mutants lacking *dcl2* (Δ*dcl2*, Δ*dcl2*Δ*aglQ*) infected by MyRV2 and MyRV1 also showed a similar accumulation pattern of vsRNAs predominantly from the positive-strand without a clear peak at the typical vsRNA size (Fig. 6). The relative number of MyRV2 vsRNA reads are higher in these mutants lacking *dcl2* compared to those in the other fungal strains (Fig. 6), which was correlated with the MyRV2 accumulation level (Fig. 3B, *SI Appendix*, Figs. S6 and S7*B*).

Taken together, these findings suggest that RnVV1 vsRNAs with a peak of 20 or 21 nt functions as virus-derived siRNA (vsiRNA) in the *C. parasitica* Dicer-alone defense in the absence of AGLs (Δ*agl2*, Δ*aglQ*, Δ*dcl2*Δ*aglQ*+*dcl2*), while RnVV1-derived sRNAs with a peak of 22 and/or 23 nt produced in *dcl2*-lacking mutants (Δ*dcl2*, Δ*dcl2*Δ*aglQ*) appears to be dysfunctional in the antiviral defense.

Discussion

This study revealed two-step antiviral RNAi in *C. parasitica*: Argonaute-independent, Dicer-mediated defense and full-scale RNAi requiring both Argonaute and Dicer (Fig. 7). Two dsRNA viruses, RnVV1 (a victorivirus) and MyRV2 (a mycoreovirus), were susceptible to the Dicer-alone defense, while CHV1 (a ssRNA hypovirus) and MyRV1 (a mycoreovirus) were not susceptible to it (Figs. 2 and 3). It is generally accepted that Dicer (DCL) is necessary but not sufficient and requires Argonaute (AGL) activity as the effector for antiviral RNAi (34). However, a Dicer-mediated, sequence-nonspecific antiviral defense has previously been discussed in plant systems (12), but it has not yet been demonstrated. The authors concluded that Argonaute is necessary in the end based

298 on several pieces of evidence, such as the observation that *agl1*/*agl2* double mutants are
299 hypersusceptible to a plant ssRNA virus, cucumber mosaic virus (12, 35). As mentioned in the
300 Introduction, it is technically difficult to fully address whether the Dicer-alone defense works for
301 some other viruses in plants or other eukaryotes because they have a large number of Argonaute
302 paralogs and the Argonaute-associated miRNA pathway is crucial for development. By contrast,
303 deletion mutants of fungal RNAi genes, even quadruple null mutants of all *agl* genes (Δ*aglQ*),
304 showed normal colony growth in the absence of virus (Fig. 4 and *SI Appendix*, Fig. S4), which led
305 to our findings in this study. This observation may suggest that *agl* genes in *C. parasitica* and possibly
306 in other ascomycetes, do not play pivotal roles in vegetative growth and development unlike in
307 other higher eukaryotes. In a model filamentous fungus, *N. crassa*, miRNA-like small RNAs
308 (milRNAs) are produced by multiple pathways (33), and one (*qde-2*) of the two argonaute genes is
309 involved in one of multiple milRNA biogenesis pathways (36). However, single or double mutants
310 of the two *N. crassa* Argonaute genes (*qde-2* and *sms-2*) show normal vegetative growth in the
311 absence of virus infection (37).
312 What determines the level of susceptibility of different viruses to the Dicer-alone defense
313 in fungi remains elusive. The interactions between host antiviral RNAi and viral counterattack,
314 more concretely *dcl2* expression levels and viral RSS activities, may partly account for this
315 phenomenon, although we cannot rule out other factors. As mentioned above, RnVV1 and MyRV2
316 were susceptible enough to be restricted by the action of DCL2 alone (Fig. 3*A* and *B*). As consistent
317 with the previous observation in strain EP155 of *C. parasitica* (31), RnVV1 accumulated at a low
318 level in DK80 in the presence of DCL2 (*SI Appendix*, Fig. S6 and S7). RnVV1 upregulated *dcl2*
319 transcript levels (Fig. 5*C* and *D*). MyRV2 is potentially able to induce *dcl2* transcription as long as
320 it can infect host fungi stably (38), while in DK80, MyRV2 cannot apparently establish stable
321 infection (*SI Appendix*, Fig. S6 and S7*B*). MyRV2 was isolated from a *C. parasitica* fungal strain co-
322 infected by a hypovirus (CHV4-C18) with a positive-sense RNA genome that encodes an RSS
323 homologous to CHV1 p29 (38, 39). MyRV2 probably needs the hypovirus for efficient suppression
324 of antiviral RNAi and for stable maintenance in the host under natural conditions (39), suggesting
325 that MyRV2 does not have a strong RSS. Similarly, RnVV1 appears to lack a strong CHV1 p29-like
326 RSS that can cancel *dcl2* induction, given that RnVV1 infection highly induces the *dcl2* transcript
327 level (Fig. 5*C* and *D*). Therefore, the susceptibility of these viruses to the Dicer-alone defense
328 appears to be equivalent to the pronounced effects of deletion of RNAi-related genes in RSS-lacking
329 viruses of other host kingdoms of host organisms (8, 40).

The stark contrast between the two sister mycoreoviruses, MyRV1 and MyRV2, in susceptibility to the Dicer-alone defense is of great interest. This difference likely led to the distinct colony phenotypes (Fig. 4), vsRNA profiles (Fig. 6), and altered gene expression (Fig. 5) between *C. parasitica* mutant strains infected by the two mycoreoviruses. Namely, MyRV1 affected colony morphology of all fungal strains, while MyRV2 induced symptoms only in the *dcl2*-lacking mutants (Δ*dcl2*, Δ*dcl2*Δ*agl2*, and Δ*dcl2*Δ*aglQ*) (Fig. 4). Furthermore, the number of differentially expressed genes including RNAi-related genes is much smaller in MyRV2-infected DK80 than in MyRV1-infected DK80 (Fig. 5). Virus-derived small RNAs were produced much less in *dcl2*-competent fungal strains infected by MyRV2 than in those infected by MyRV1 (Fig. 6). No Dicer-alone defense against MyRV1 was discernable regardless of the presence or absence of *agl2* (Fig. 3*C*), suggesting its tolerance to antiviral RNAi, despite the high *dcl2* induction (Figs. 3*F* and 5*D*). The genus *Mycorevirus* accommodates another member Rosellinia necatrix mycoreovirus 3 (MyRV3) as well as the above two mycoreoviruses (41). One of the MyRV3-encoded proteins, VP10, was identified as an RSS (42), but no homologous protein is detected in MyRV1 or MyRV2. Future comparative functional analyses of the genomic segments homologous between MyRV1 and MyRV2 will provide some clues.

This study provides insights into the functional roles of Argonaute family members. Fungal Argonaute homologs (AGL) are largely divided into two groups, the so-called quelling and meiotic silencing by unpaired DNA (MSUD) clades, based on the phylogenetic affinity to the two Argonaute proteins, QDE2 (quelling-defective 2) and SMS2 (suppressor of meiotic silencing-2), of the model filamentous fungus *N. crassa* (43). In *N. crassa*, QDE2 and SMS2 work in the vegetative and sexual stages, respectively (44, 45), and QDE2, but not SMS2, contributes to viral RNA reduction in the vegetative growth condition (37). Similarly to QDE2, all antiviral Argonaute proteins from various filamentous fungi belong to the same quelling clade, as exemplified by AGL2 in *C. parasitica* (46). There are a few exceptions to this with phytopathogenic fungi, including FgAGO2 (a MSUD clade member) from *Fusarium graminearum* (46, 47). Both FgAGO1 (a quelling clade member) and FgAGO2, whose genes are induced upon virus infection, play antiviral roles (47). The second example is from *Magnaporthe oryzae* that carries three Argonaute paralogs. MoAGO2 and MoAGO3, which belong to the quelling clade, exert contrasting effects: MoAGO3 contributes to viral RNA reduction, whereas MoAGO2 functions as a proviral factor likely by competing with antiviral MoAGO3 over vsiRNA binding (48). Other functional roles of MoAGO2 remain unknown. Much simpler antiviral RNAi appears to operate in *C. parasitica*, in which only DCL2 and AGL2 are

functional (10, 21, 23). Their genes (*dcl2* and *agl2*) are upregulated upon virus infection at the vegetative stage on medium to a much higher extent than *dcl1*, *agl1*, *agl3*, and *agl4*, which were not induced by the tested viruses (Fig. 5*C* and *D*). It should be noted that *agl1*, *agl3*, and *agl4* are upregulated in sexual fruiting bodies of *C. parasitica* on its natural host plant (chestnut) (21), so the antiviral contribution of these *agl* genes in untested conditions (e.g., at sexual stage) remains to be determined. The antiviral roles of *C. parasitica dcl2* and *agl2* in the tested conditions appear to require their appropriate temporal and spatial expression.

Eukaryotic antiviral RNAi has been proposed to have evolved from the prokaryotic/archaeal Argonaute-mediated antiviral mechanism, in which Dicer is not involved (1, 49), implying that Argonaute precedes Dicer on an evolutionary time scale. Dicer is hypothesized to have evolved by fusion of prokaryotic RNase III and archaeal helicase (50). RNase III family proteins are structurally classified into three classes, where Dicer belongs to class III (51). Besides Dicer, Drosha, a class II type of RNase III family protein, also plays a role in miRNA processing (52) and serves as a direct antiviral effector, independent of miRNA (53). Conceptionally, the second role somewhat resembles the direct antiviral effect of Dicer observed in this study. However, Drosha exerts its antiviral activity by binding to viral RNA and inhibiting viral RNA synthesis through viral RdRP (53), while the antiviral effect of Dicer discovered in this study is likely attributed to its dicing of viral-derived dsRNA based on the vsiRNA production (Fig. 6). In this regard, the Dicer-alone antiviral defense is more similar to the antiviral defense mediated by the 5′→3′ cytoplasmic exoribonuclease, which was first observed in the budding yeast *Saccharomyces cerevisiae* (54-56) and later in various eukaryotes such as mammals (57) and plants (58). The Dicer-alone antiviral RNA defense we discovered in this study resembles these defense mechanisms in that the effector molecules have nuclease activities in a sequence-nonspecific manner. The Argonaute-independent, Dicer-dependent antiviral defense may require high levels of Dicer accumulation induced by virus infection or dsRNA (21, 23, 59), which may be functionally equivalent to the RdRP-mediated siRNA amplification circuit in plants (22).

Materials and Methods

The viral and fungal strains used in this study are listed in Table 1 and *SI Appendix*, Table S3. The fungal strains were grown on potato dextrose agar (PDA) (BD Difco) on laboratory shelves at room temperature in natural daylight. Disruptants of *C. parasitica* RNAi genes were basically prepared via homologous recombination-mediated gene replacement, and validated by genomic PCR and

Southern blotting (Fig. 1*B* and *SI Appendix*, Figs. S1-S3). Virus inoculation was conducted by conventional virion transfection or coculturing of donor and recipient fungal strains (25, 31). RNA isolation and subsequent analyses were performed as described earlier (25, 31). All detailed protocols and materials are described in *SI Appendix*, Materials and Methods. Any materials or related protocols mentioned in this work can be obtained by contacting the corresponding author upon request.

Data, Materials, and Software Availability. The genome sequence and gene annotation of *C. parasitica* is available in genome portal Cryphonectria parasitica EP155 v2.0 (https://mycocosm.jgi.doe.gov/Crypa2) organized by Joint Genome Institute (60). Gene and viral sequences are available under the accession numbers listed in Table S2. All other data are available in the manuscript and the supplementary material.

ACKNOWLEDGMENTS. This study was supported in part by Yomogi Inc. (to N.S.), and Grants-in-Aid for Scientific Research (A and B) and on Innovative Areas, and Grants-in-Aid for Research Activity Start-up from the Japanese Ministry of Education, Culture, Sports, Science, and Technology (MEXT) (KAKENHI 22F22095, 21H05035, 21K18222, 16H06436, 16H06429, and 16K21723 to N.S. and HK, and 19J00261 to Y.S.). The fungal strains 9B21/MyRV1, C18/MyRV2, EP155, EP155/CHV1, and EP155/CHV1-Δp69 were generous gifts from Dr. Donald L. Nuss and Bradley I Hillman. The fungal strain DK80 were generously provided by Bao-shan Chen (Guangxi University, China). The plasmid vectors pKAES175, pAL12-Lifeact, or pCB1636_lox_HPT-TK were generously provided by Dr. Christopher L. Schardl (University of Kentucky), Dr. Shinji Honda (University of Fukui, Japan), or Dr. Koji Yamada (Tokushima University, Japan), respectively. The authors are grateful to Ms Sakae Hisano and Dr. Annisa Aulia for their excellent technical support for qRT-PCR and preparation of the fungal strains (EP155Δ*dcl2*/MyRV2 and EP155/CHV4), respectively.

Author contributions: NS, YS. Conceptualization; YS, HK. Methodology; YS, HK, NS. Investigation; YS, HK. Visualization; NS, YS, HK. Funding acquisition; YS, NS. Writing – original draft; YS, HK, NS. Writing – review & editing

Competing interests: The authors declare no competing interests.

REFERENCES

1. B. R. tenOever, The Evolution of Antiviral Defense Systems. *Cell Host Microbe* **19**, 142-149 (2016).
2. R. Aliyari, S. W. Ding, RNA-based viral immunity initiated by the Dicer family of host immune receptors. *Immunol Rev* **227**, 176-188 (2009).
3. D. C. Baulcombe, The role of viruses in identifying and analyzing RNA silencing. *Annu Rev Virol* **9**, 353-373 (2022).
4. D. L. Nuss, Mycoviruses, RNA silencing, and viral RNA recombination. *Adv Virus Res* **80**, 25-48 (2011).
5. Z. Guo, Y. Li, S. W. Ding, Small RNA-based antimicrobial immunity. *Nat Rev Immunol* **19**, 31-44 (2019).
6. M. Ghildiyal, P. D. Zamore, Small silencing RNAs: an expanding universe. *Nat Rev Genet* **10**, 94-108 (2009).
7. O. Voinnet, Use, tolerance and avoidance of amplified RNA silencing by plants. *Trends in Plant Science* **13**, 317-328 (2008).
8. X. H. Wang *et al.*, RNA interference directs innate immunity against viruses in adult *Drosophila*. *Science* **312**, 452-454 (2006).
9. H. Garcia-Ruiz *et al.*, *Arabidopsis* RNA-dependent RNA polymerases and dicer-like proteins in antiviral defense and small interfering RNA biogenesis during *Turnip Mosaic Virus* infection. *Plant Cell* **22**, 481-496 (2010).
10. G. C. Segers, X. Zhang, F. Deng, Q. Sun, D. L. Nuss, Evidence that RNA silencing functions as an antiviral defense mechanism in fungi. *Proc Natl Acad Sci U S A* **104**, 12902-12906 (2007).
11. P. Mourrain *et al.*, *Arabidopsis* SGS2 and SGS3 genes are required for posttranscriptional gene silencing and natural virus resistance. *Cell* **101**, 533-542 (2000).
12. N. Pumplin, O. Voinnet, RNA silencing suppression by plant pathogens: defence, counter-defence and counter-counter-defence. *Nat Rev Microbiol* **11**, 745-760 (2013).
13. X. Fang, Y. Qi, RNAi in plants: An Argonaute-centered view. *Plant Cell* **28**, 272-285 (2016).
14. E. Wienholds, R. H. Plasterk, MicroRNA function in animal development. *FEBS Lett* **579**, 5911-5922 (2005).
15. J. B. Morel *et al.*, Fertile hypomorphic *ARGONAUTE* (*ago1*) mutants impaired in post-transcriptional gene silencing and virus resistance. *Plant Cell* **14**, 629-639 (2002).
16. T. Sasaki, A. Shiohama, S. Minoshima, N. Shimizu, Identification of eight members of the Argonaute family in the human genome. *Genomics* **82**, 323-330 (2003).
17. R. W. Williams, G. M. Rubin, *ARGONAUTE1* is required for efficient RNA interference in *Drosophila* embryos. *Proc Natl Acad Sci USA* **99**, 6889-6894 (2002).
18. E. Yigit *et al.*, Analysis of the *C. elegans* argonaute family reveals that distinct argonautes act sequentially during RNAi. *Cell* **127**, 747-757 (2006).
19. D. Rigling, S. Prospero, *Cryphonectria parasitica*, the causal agent of chestnut blight: invasion history, population biology and disease control. *Mol Plant Pathol* **19**, 7-20 (2018).
20. A. Eusebio-Cope *et al.*, The chestnut blight fungus for studies on virus/host and virus/virus interactions: From a natural to a model host. *Virology* **477**, 164-175 (2015).
21. Q. Sun, G. H. Choi, D. L. Nuss, A single Argonaute gene is required for induction of RNA silencing antiviral defense and promotes viral RNA recombination. *Proc Natl Acad Sci U S A* **106**, 17927-17932 (2009).
22. D. X. Zhang, M. J. Spiering, D. L. Nuss, Characterizing the roles of *Cryphonectria parasitica* RNA-dependent RNA polymerase-like genes in antiviral defense, viral recombination and transposon transcript accumulation. *PLoS One* **9**, e108653 (2014).
23. S. Chiba, N. Suzuki, Highly activated RNA silencing via strong induction of dicer by one virus

can interfere with the replication of an unrelated virus. *Proc Natl Acad Sci U S A* **112**, E4911-E4918 (2015).
24. A. Aulia, M. Tabara, P. Telengech, T. Fukuhara, N. Suzuki, Dicer monitoring in a model filamentous fungus host, *Cryphonectria parasitica*. *Curr Res Virol Sci* **1**, 100001 (2020).
25. I. B. Andika, H. Kondo, N. Suzuki, Dicer functions transcriptionally and post-transcriptionally in a multilayer antiviral defense. *Proc Natl Acad Sci U S A* **116**, 2274-2281 (2019).
26. I. B. Andika, A. Jamal, H. Kondo, N. Suzuki, SAGA complex mediates the transcriptional up-regulation of antiviral RNA silencing. *Proc Natl Acad Sci U S A* **114**, E3499-E3506 (2017).
27. X. Zhang, G. C. Segers, Q. Sun, F. Deng, D. L. Nuss, Characterization of hypovirus-derived small RNAs generated in the chestnut blight fungus by an inducible DCL-2-dependent pathway. *J Virol* **82**, 2613-2619 (2008).
28. D. C. Swarts *et al.*, The evolutionary journey of Argonaute proteins. *Nat Struct Mol Biol* **21**, 743-753 (2014).
29. X. Lan *et al.*, Deletion of the *cpku80* gene in the chestnut blight fungus, *Cryphonectria parasitica*, enhances gene disruption efficiency. *Curr Genet* **53**, 59-66 (2008).
30. D. X. Zhang, H. L. Lu, X. Liao, R. J. St Leger, D. L. Nuss, Simple and efficient recycling of fungal selectable marker genes with the Cre-*loxP* recombination system via anastomosis. *Fungal Genet Biol* **61**, 1-8 (2013).
31. S. Chiba, Y. H. Lin, H. Kondo, S. Kanematsu, N. Suzuki, A novel victorivirus from a phytopathogenic fungus, *Rosellinia necatrix* is infectious as particles and targeted by RNA silencing. *J Virol* **87**, 6727-6738 (2013).
32. X. Zhang, D. L. Nuss, A host dicer is required for defective viral RNA production and recombinant virus vector RNA instability for a positive sense RNA virus. *Proc Natl Acad Sci U S A* **105**, 16749-16754 (2008).
33. H. C. Lee *et al.*, Diverse pathways generate microRNA-like RNAs and Dicer-independent small interfering RNAs in fungi. *Mol Cell* **38**, 803-814 (2010).
34. G. Silva-Martins, A. Bolaji, P. Moffett, What does it take to be antiviral? An Argonaute-centered perspective on plant antiviral defense. *J Exp Bot* **71**, 6197-6210 (2020).
35. X. B. Wang *et al.*, The 21-nucleotide, but not 22-nucleotide, viral secondary small interfering RNAs direct potent antiviral defense by two cooperative argonautes in *Arabidopsis thaliana*. *Plant Cell* **23**, 1625-1638 (2011).
36. Z. Xue, H. Yuan, J. Guo, Y. Liu, Reconstitution of an Argonaute-dependent small RNA biogenesis pathway reveals a handover mechanism involving the RNA exosome and the exonuclease QIP. *Mol Cell* **46**, 299-310 (2012).
37. S. Honda *et al.*, Establishment of *Neurospora crassa* as a model organism for fungal virology. *Nature Communications* **11**, 5627 (2020).
38. A. Aulia, I. B. Andika, H. Kondo, B. I. Hillman, N. Suzuki, A symptomless hypovirus, CHV4, facilitates stable infection of the chestnut blight fungus by a coinfecting reovirus likely through suppression of antiviral RNA silencing. *Virology* **533**, 99-107 (2019).
39. A. Aulia *et al.*, Identification of an RNA silencing suppressor encoded by a symptomless fungal hypovirus, Cryphonectria hypovirus 4. *Biology (Basel)* **10**, 100 (2021).
40. R. Aliyari *et al.*, Mechanism of induction and suppression of antiviral immunity directed by virus-derived small RNAs in *Drosophila*. *Cell Host Microbe* **4**, 387-397 (2008).
41. J. Matthijnssens *et al.*, ICTV Virus Taxonomy Profile: *Spinareoviridae* 2022. *J Gen Virol* **103**, 001781 (2022).
42. H. Yaegashi, N. Yoshikawa, T. Ito, S. Kanematsu, A mycoreovirus suppresses RNA silencing in the white root rot fungus, *Rosellinia necatrix*. *Virology* **444**, 409-416 (2013).
43. S. Campo, K. B. Gilbert, J. C. Carrington, Small RNA-Based Antiviral Defense in the Phytopathogenic Fungus *Colletotrichum higginsianum*. *PLoS Pathog* **12**, e1005640 (2016).
44. C. Cogoni, G. Macino, Isolation of quelling-defective (*qde*) mutants impaired in

posttranscriptional transgene-induced gene silencing in *Neurospora crassa*. *Proc Natl Acad Sci U S A* **94**, 10233-10238 (1997).
45. D. W. Lee, R. J. Pratt, M. McLaughlin, R. Aramayo, An argonaute-like protein is required for meiotic silencing. *Genetics* **164**, 821-828 (2003).
46. Y. Sato, N. Suzuki, Continued mycovirus discovery expanding our understanding of virus lifestyles, symptom expression, and host defense. *Current Opinion in Microbiology* **75**, 102337 (2023).
47. J. Yu, K. M. Lee, W. K. Cho, J. Y. Park, K. H. Kim, Differential contribution of RNA interference components in response to distinct *Fusarium graminearum* virus infections. *J Virol* **92**, e01756-01717 (2018).
48. Q. Nguyen *et al.*, A fungal Argonaute interferes with RNA interference. *Nucleic Acids Res* **46**, 2495-2508 (2018).
49. E. V. Koonin, Evolution of RNA- and DNA-guided antivirus defense systems in prokaryotes and eukaryotes: common ancestry vs convergence. *Biol Direct* **12**, 5 (2017).
50. S. A. Shabalina, E. V. Koonin, Origins and evolution of eukaryotic RNA interference. *Trends Ecol Evol* **23**, 578-587 (2008).
51. M. A. Carmell, G. J. Hannon, RNase III enzymes and the initiation of gene silencing. *Nat Struct Mol Biol* **11**, 214-218 (2004).
52. J. Han *et al.*, The Drosha-DGCR8 complex in primary microRNA processing. *Genes Dev* **18**, 3016-3027 (2004).
53. L. C. Aguado *et al.*, RNase III nucleases from diverse kingdoms serve as antiviral effectors. *Nature* **547**, 114-117 (2017).
54. A. Toh-e, P. Guerry, R. B. Wickner, Chromosomal superkiller mutants of *Saccharomyces cerevisiae*. *J Bacteriol* **136**, 1002-1007 (1978).
55. R. Esteban, L. Vega, T. Fujimura, 20S RNA narnavirus defies the antiviral activity of SKI1/XRN1 in *Saccharomyces cerevisiae*. *J Biol Chem* **283**, 25812-25820 (2008).
56. R. B. Wickner, "Viruses and prions of yeasts, fungi, and unicellular organisms" in Fields Virology 7th Edition, D. M. a. H. Knipe, P., Ed. (Wolster Kluwer, Philadelphia, 2023), vol. 4.
57. Y. Li, T. Masaki, D. Yamane, D. R. McGivern, S. M. Lemon, Competing and noncompeting activities of miR-122 and the 5' exonuclease Xrn1 in regulation of hepatitis C virus replication. *Proc Natl Acad Sci U S A* **110**, 1881-1886 (2013).
58. F. F. Li, A. M. Wang, RNA decay is an antiviral defense in plants that is counteracted by viral RNA silencing suppressors. *PloS Pathog* **14**, e1007228 (2018).
59. S. Choudhary *et al.*, A double-stranded-RNA response program important for RNA interference efficiency. *Mol Cell Biol* **27**, 3995-4005 (2007).
60. J. A. Crouch *et al.*, Genome sequence of the chestnut blight fungus *Cryphonectria parasitica* EP155: A fundamental resource for an archetypical invasive plant pathogen. *Phytopathology* **110**, 1180-1188 (2020).
61. R. Shapira, G. H. Choi, D. L. Nuss, Virus-like genetic organization and expression strategy for a double-stranded RNA genetic element associated with biological control of chestnut blight. *EMBO J* **10**, 731-739 (1991).
62. N. Suzuki, S. Supyani, K. Maruyama, B. I. Hillman, Complete genome sequence of Mycoreovirus-1/Cp9B21, a member of a novel genus within the family *Reoviridae*, isolated from the chestnut blight fungus *Cryphonectria parasitica*. *J Gen Virol* **85**, 3437-3448 (2004).
63. S. A. Enebak, W. L. Macdonald, B. I. Hillman, Effect of dsRNA associated with Isolates of *Cryphonectria parasitica* from the central Appalachians and their relatedness to other dsRNA from North America and Europe. *Phytopathology* **84**, 528-534 (1994).
64. N. Suzuki, D. L. Nuss, Contribution of protein p40 to hypovirus-mediated modulation of fungal host phenotype and viral RNA accumulation. *J Virol* **76**, 7747-7759 (2002).
65. B. I. Hillman, R. Shapira, D. L. Nuss, Hypovirulence-associated suppression of host function in

Cryphonectria parasitica can be partially relieved by high-light intesity *Phytopathology* **80**, 950-956 (1990).

66. A. Eusebio-Cope, N. Suzuki, Mycoreovirus genome rearrangements associated with RNA silencing deficiency. *Nucleic Acids Res* **43**, 3802-3813 (2015).

SUPPLEMETAL INFORMATION

Materials and Methods

Supplementary Figs. S1 to S8

Tables S1 to S4

References (*1–36*)

Figure legends

Fig. 1: Disruption of Argonaute-like protein genes (*agl*) with Dicer-like protein genes (*dcl*) in *Cryphonectria parasitica*. **(*A*)** Four Argonaute-like proteins (AGLs) of *C. parasitica* DK80, a *ku80*-deletion mutant of a reference strain EP155. These AGLs collectively include six typical Argonaute domains, namely Argonaute linker 1 domain (ArgoL1), Argonaute linker 2 domain (ArgoL2), mid domain of Argonaute (ArgoMid), N-terminal domain of Argonaute (ArgoN), PAZ domain (PAZ), and Piwi domain (Piwi) (Pfam accession: PF08699.13, PF16488.8, PF16487.8, PF16486.8, PF02170.25, and PF02171.20, respectively). **(*B*)** Single or multiple deletions of dicer-like protein genes (*dcl1* and *dcl2*) and/or argonaute-like protein genes (*agl1*, *agl2*, *agl3*, and *agl4*), validated by polymerase chain reaction (PCR). The strain names of *C. parasitica* mutants lacking *dcl2* are displayed in red, while those lacking *agl2* but possessing *dcl2* are shown in blue in the left panel. Other singlet mutants (Δ*dcl1*, Δ*agl1,* Δ*agl3* and Δ*agl4*) are shown in the right panel. Agarose gels were stained with ethidium bromide (EtBr). The PCR targets regions removed by homologous recombination within two *dcl* and four *agl* genes (*SI Appendix*, Fig. S1). The actin gene (*act*) was detected as a positive control of PCR templates (genomic DNA of each fungal strain). Expected amplicon sizes from the intact genes are provided in the Supplementary Information (*SI Appendix*, Table S2).

Fig. 2: Viral RNA accumulation in the *dcl/agl* single knockout strains of *Cryphonectria parasitica*.

(*A*) The viral inoculation method via hyphal fusion. For the detailed procedure, refer to the Methods section. **(*B*, *C*)** Detection of RnVV1 (*B*) or CHV1 (*C*) RNA in virus-free or virus-infected fungal mycelia by northern hybridization. Each virus was inoculated via hyphal fusion. Northern hybridization was carried out with crude RNA enriched with ssRNA by lithium chloride (LiCl). In all northern hybridization, host ribosomal RNA (rRNA) with ethidium bromide (EtBr) staining is shown as a loading control. CHV1 was detected with a probe targeting a region lost in the major

CHV1 DI RNA (32). Red arrows indicate the position of viral full-length mRNA and/or genomic RNA. (***D***) Viral inoculation for a heterologous virus (RnVV1) via virion transfection. For the detailed procedure, refer to the Methods section. (***E***) Detection of RnVV1 RNA in virus-free or RnVV1-infected fungal mycelia by semi-quantitative reverse transcription–polymerase chain reaction (semi-qRT-PCR) and northern hybridization with LiCl-precipitated ssRNA fractions. RnVV1 was inoculated by virion transfection. Relative band intensity values for semi-qRT-PCR are shown below the electrophoretic image. ND stands for not determined/detected.

Fig. 3: Viral RNA accumulation and *dcl2*/*agl2* induction in the *dcl2/agl* single and multiple knockout strains of *Cryphonectria parasitica*.

(***A–E***) Detection of viruses in total RNA extracted from the host strains. Each of RnVV1 (***A***), MyRV2 (***B***), MyRV1 (***C***), CHV1 (***D***), and CHV1-Δp69 (***E***) was inoculated to the fungal strains and the respective viruses were detected in parallel with virus-free fungal strains as negative controls. For each of (***A***)-(***E***), the upper row indicates fungal total RNA (DNase-treated total nucleic acids) with or without viral RNA detected by ethidium bromide (EtBr) staining, while the lower row of each panel indicates the blots with viral signals detected by northern hybridization of the total RNA. The fungal strains lacking *dcl2* are indicated with red. The fungal strains lacking *agl2* but possessing *dcl2* are indicated with blue. The other fungal strains are indicated with black. Same for the following panels (***F***, ***G***). The red arrow indicates the position of the genome or its replicative form dsRNA of non-segmented viruses (RnVV1, CHV1, and CHV1-Δp69) or the RdRP-encoding segment of multi-segmented viruses (MyRV1 and MyRV2, the smaller viral bands are the other segments). The letter "r" indicates fungal ribosomal RNA (rRNA) bands as internal loading controls. "D1," and "D2" represent an RNAi-dependent DI RNA (32) and an RNAi-independent defective RNA of CHV1, respectively. (***F***, ***G***) Detection of *dcl2*/*agl2* mRNA by northern hybridization with LiCl-precipitated RNA fractions. To test the induction of *dcl2* and *agl2* in the respective fungal strains upon virus infection, we used MyRV1 (***F***) or CHV1-Δp69 (***G***) which are known to induce *dcl2* and *agl2* expression in wild-type fungal strains. Host rRNA (r) is shown as a loading control.

Fig. 4: Viral symptoms in the *dcl2/agl* single and multiple knockout strains of *Cryphonectria parasitica*. DK80 and its mutants infected by each virus or no virus (Fig. 3*A–E*) were cultured on potato dextrose agar (5.5 cm in diameter) for 5 days after a small (1 mm^3) mycelial plug was placed onto the center of each plate.

644

645 **Fig. 5. Virus-induced transcriptomic changes in *Cryphonectria parasitica*.** The transcriptomes of
646 *C. parasitica* strains DK80 and Δ*dcl2,* which received each virus by hyphal fusion, were analyzed
647 with virus-free strains as a control. There were two independent virus inoculations, representing
648 two biological replicates of the transcriptomes. **(*A*)** Principle component (PC) analysis of the
649 transcriptomes. **(*B*)** The count of upregulated genes [adjusted *p* value (*padj*) < 0.05, $\log_2$ fold change
650 ($\log_2$ FC) > 0] or downregulated genes (*padj* < 0.05, $\log_2$ FC < 0) upon virus infection among a total
651 of 11609 genes. **(*C*)** The heat map of the expression level of RNAi-related genes, namely *rdr*
652 (encoding host RNA-dependent RNA polymerase), *dcl*, and *agl* (*SI Appendix*, Table S4). The
653 expression level is shown as transcripts per million (TPM) plus one converted to the $\log_{10}$ scale. **(*D*)**
654 The heat map of $\log_2$ FC of the RNAi-related genes induced by each virus. $^{*}p < 0.05$ but $padj \geq 0.05$.
655 ** $padj < 0.05$.
656

657 **Fig. 6: Accumulation of virus-derived small RNA (vsRNA) in the *dcl2/agl* single and multiple**
658 **knockout strains of *Cryphonectria parasitica*.** The *x*-axis shows size distributions (16-30 nt) of
659 RnVV1-, MyRV2-, MyRV1-, or CHV1-derived vsRNAs. The *y*-axis shows normalized vsRNA read
660 counts [reads per million (RPM) divided by 1000, normalized to total small RNAs in *C. parasitica*
661 strain DK80 or its derivative mutants (Δ*dcl2*, Δ*agl2*, Δ*aglQ*, Δ*dcl2*Δ*aglQ*, and Δ*dcl2*Δ*aglQ*+*dcl2*)
662 infected by each virus].
663

664 **Fig. 7. Schematic representation of Argonaute-independent antiviral silencing.** In canonical
665 antiviral silencing/RNAi (left panel), Dicer (or DCL) dices viral dsRNA into vsiRNAs, and then
666 Argonaute (or AGL) incorporates the vsiRNA to slice or translationally repress the target viral
667 ssRNA. In this case, both Dicer and Argonaute could contribute to the inhibition of viral replication.
668 In contrast, this study also suggests that infection of some viruses (RnVV1 and MyRV2) can be
669 suppressed in an Argonaute-independent manner (right panel), by dicing of viral
670 replicative/genomic dsRNA to block the replication cycle of RNA viruses in the realm *Riboviria*.
671

672 **Table 1.** Viral and fungal strains used in this study[a]

Strain	Description	Reference
Viral		
CHV1	Non-segmented, positive-sense RNA virus (12734 nt) in the genus *Hypovirus* in the family *Hypoviridae*, from *C. parasitica* strain EP713	(61)
RnVV1	Non-segmented dsRNA virus (5329 bp) in the genus *Victorivirus* in the family *Totiviridae*, from *R. necatrix* strain W1029	(31)
MyRV1	Eleven-segmented dsRNA virus (732-4127 bp segments) in the genus *Mycoreovirus* in the family *Spinareoviridae*, from *C. parasitica* strain 9B21	(62)
MyRV2	Eleven-segmented dsRNA virus[c] in the genus *Mycoreovirus* in the family *Spinareoviridae*, from *C. parasitica* strain C18	(63)
CHV1-Δp69	A CHV1 mutant lacking ORFA that encodes p69, a precursor of RSS p29	(64)
Fungal		
EP155	A standard virus-free strain of *C. parasitica*	(60)
EP155/CHV1	*C. parasitica* EP155 inoculated with CHV1 isolate EP713	(65)
EP155Δ*dcl2*/RnVV1	*C. parasitica* EP155 Δ*dcl2* inoculated with RnVV1 isolate W1029	(31)
EP155/MyRV1	*C. parasitica* EP155 inoculated with MyRV1 isolate 9B21	(66)
EP155Δ*dcl2*/MyRV2	*C. parasitica* EP155 Δ*dcl2* inoculated with MyRV2 isolate C18	This study
EP155/CHV1-Δp69	*C. parasitica* EP155 inoculated with CHV1-Δp69	(64)
DK80	*cpku80* knockout strain in *C. parasitica* EP155 background	(29)
Δ*dcl1*[b]	*dcl1* knockout strain in *C. parasitica* DK80 background	This study
Δ*dcl2*[b]	*dcl2* knockout strain in *C. parasitica* DK80 background	This study
Δ*agl1*[b]	*agl1* knockout strain in *C. parasitica* DK80 background	This study
Δ*agl2*[b]	*agl2* knockout strain in *C. parasitica* DK80 background	This study
Δ*agl3*[b]	*agl3* knockout strain in *C. parasitica* DK80 background	This study
Δ*agl4*[b]	*agl4* knockout strain in *C. parasitica* DK80 background	This study
Δ*dcl2*Δ*agl2*	*dcl2* and *agl2* knockout strain in *C. parasitica* DK80 background	This study
Δ*agl1/3/4*	*agl1*, *agl3*, and *agl4* knockout strain in *C. parasitica* DK80 background	This study
Δ*aglQ*	Quadruple *agl* (*agl1* to *agl4*) knockout strain in *C. parasitica* DK80 background	This study
Δ*dcl2*Δ*aglQ*	*dcl2* knockout strain in *C. parasitica* DK80 Δ*aglQ* background	This study
Δ*dcl2*Δ*aglQ+dcl2*	*dcl2* complementation strain of *C. parasitica* DK80 Δ*dcl2*Δ*aglQ*	This study

673

674 [a] Viral and fungal strains used only in the supplementary data are listed in *SI Appendix*, Table S3.

675 [b] Knockout strains newly generated in DK80 background, different from the previously generated ones

676 in EP155 background (10, 21).

677 [c] The sequence of dsRNA3 (3213 bp) is available in GenBank (accession: DQ902580).

678

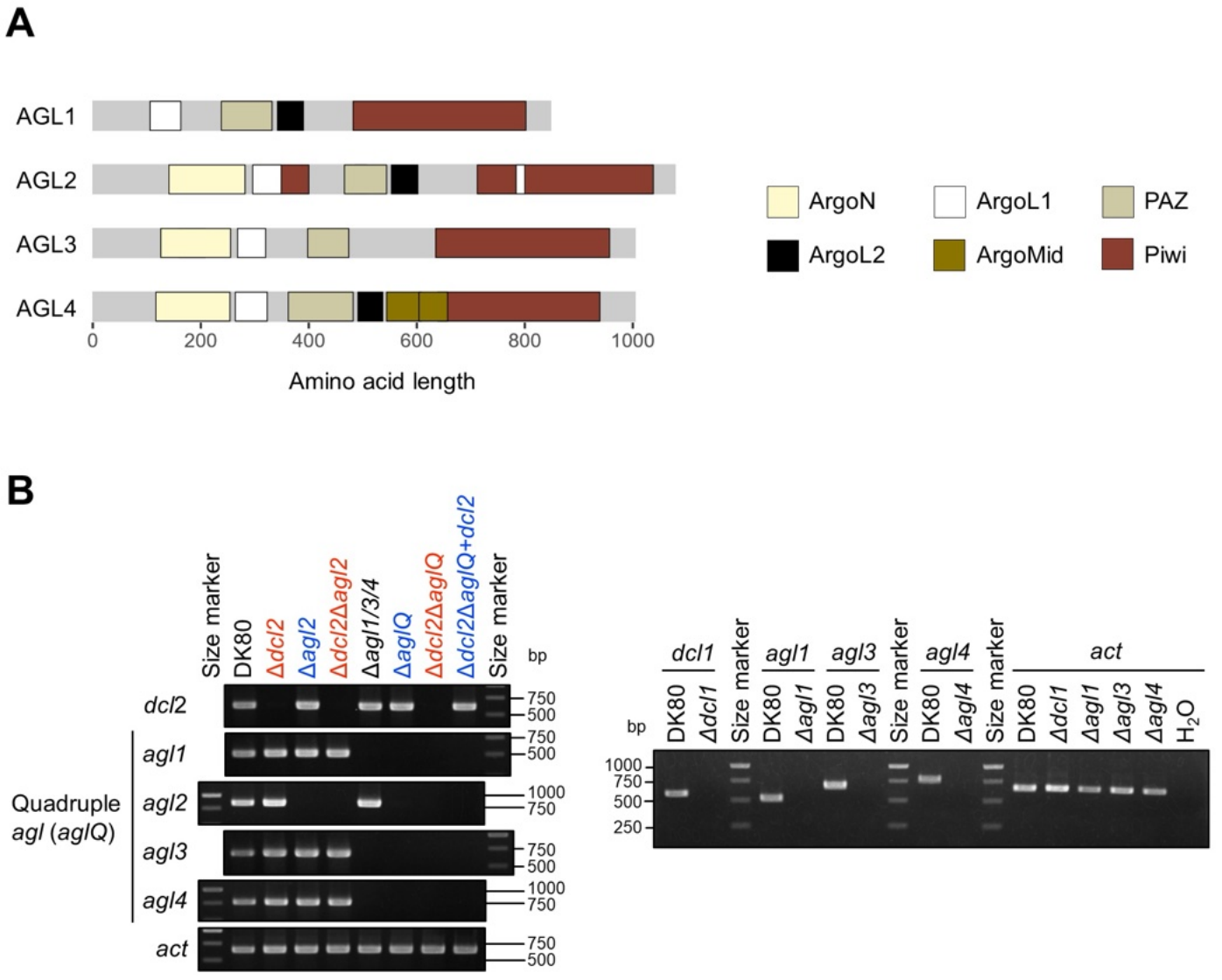
A
AGL1
AGL2
AGL3
AGL4
0
200
400
600
800
1000
Amino acid length
ArgoN
ArgoL1
PAZ
ArgoL2
ArgoMid
Piwi
B
Size marker
DK80
Δdcl2
Δagl2
Δdcl2Δagl2
Δagl1/3/4
ΔaglQ
Δdcl2ΔaglQ
Δdcl2ΔaglQ+dcl2
Size marker
bp
dcl2
agl1
agl2
agl3
agl4
act
Quadruple agl (aglQ)
750
500
1000
750
dcl1
agl1
agl3
agl4
act
Δdcl1
Δagl1
Δagl3
Δagl4
H2O
1000
750
500
250

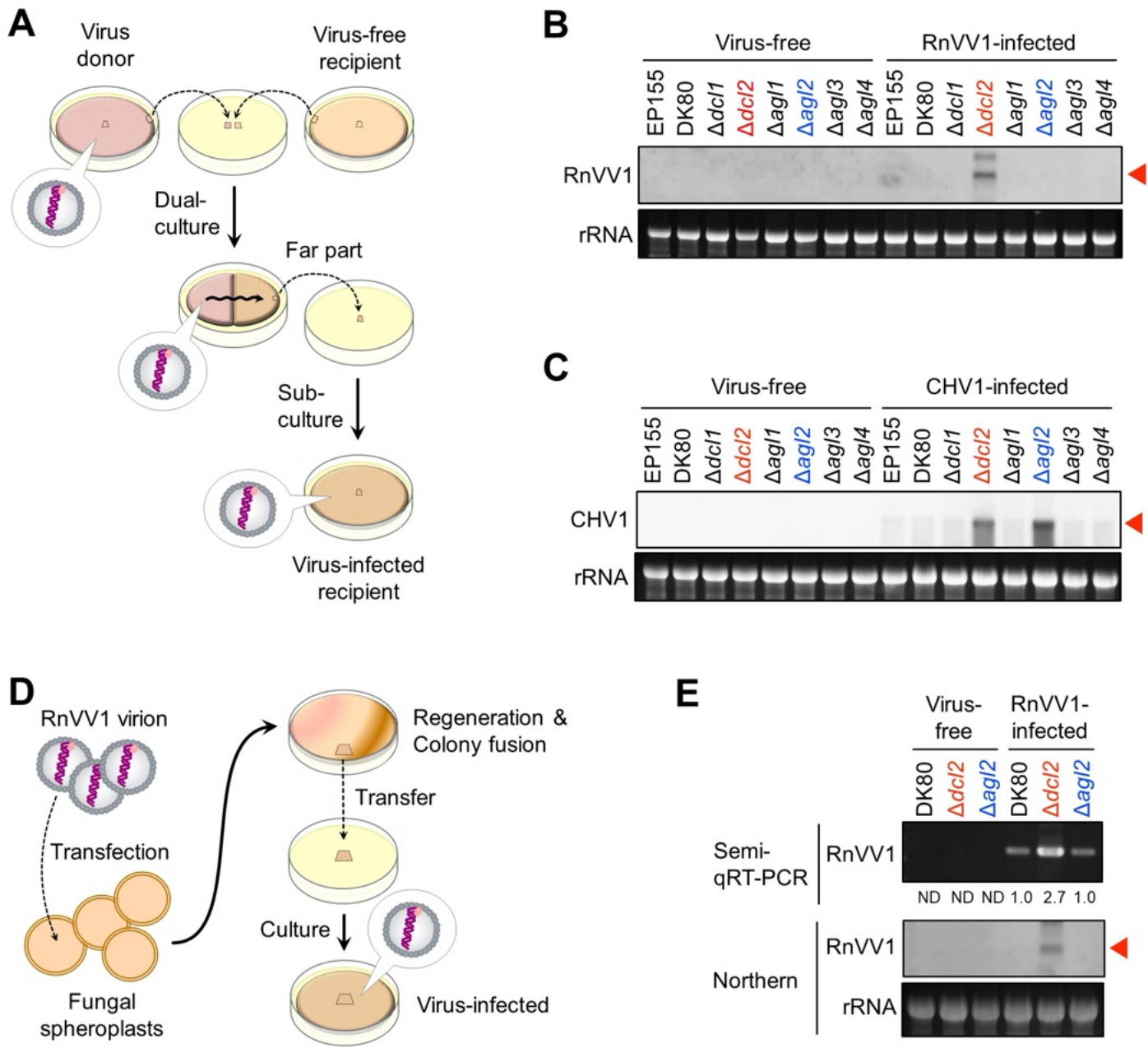
A
Virus donor
Virus-free recipient
Dual-culture
Far part
Sub-culture
Virus-infected recipient
B
Virus-free
RnVV1-infected
EP155
DK80
Δdcl1
Δdcl2
Δagl1
Δagl2
Δagl3
Δagl4
RnVV1
rRNA
C
Virus-free
CHV1-infected
CHV1
rRNA
D
RnVV1 virion
Transfection
Fungal spheroplasts
Regeneration & Colony fusion
Transfer
Culture
Virus-infected
E
Virus-free
RnVV1-infected
Semi-qRT-PCR
RnVV1
ND ND ND 1.0 2.7 1.0
Northern
RnVV1
rRNA

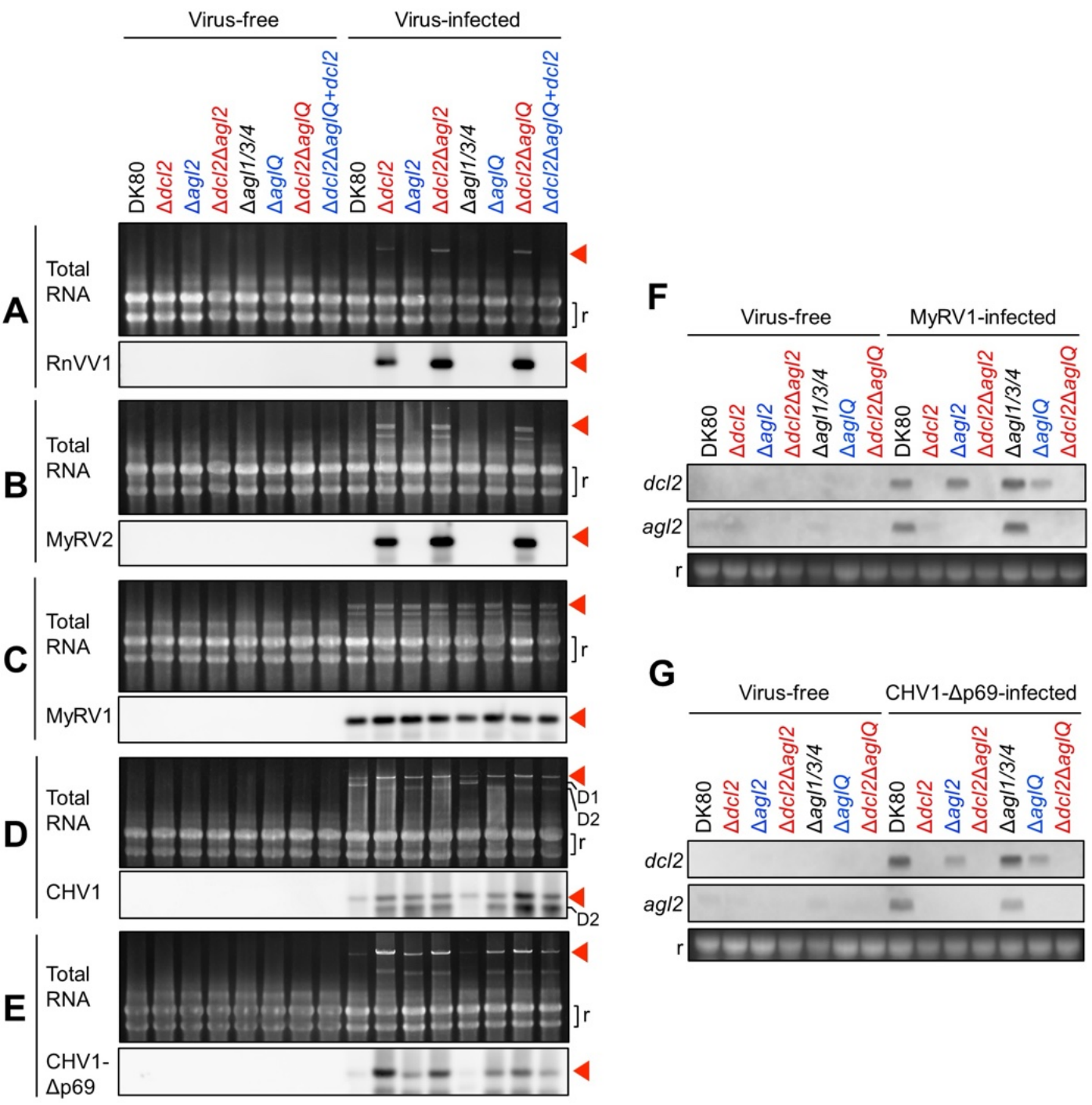
Virus-free
Virus-infected
DK80
Δdcl2
Δagl2
Δdcl2Δagl2
Δagl1/3/4
ΔaglQ
Δdcl2ΔaglQ
Δdcl2ΔaglQ+dcl2
A
Total RNA
RnVV1
B
Total RNA
MyRV2
C
Total RNA
MyRV1
D
Total RNA
CHV1
D1
D2
D2
E
Total RNA
CHV1-Δp69
]r
F
Virus-free
MyRV1-infected
dcl2
agl2
r
G
Virus-free
CHV1-Δp69-infected
dcl2
agl2
r

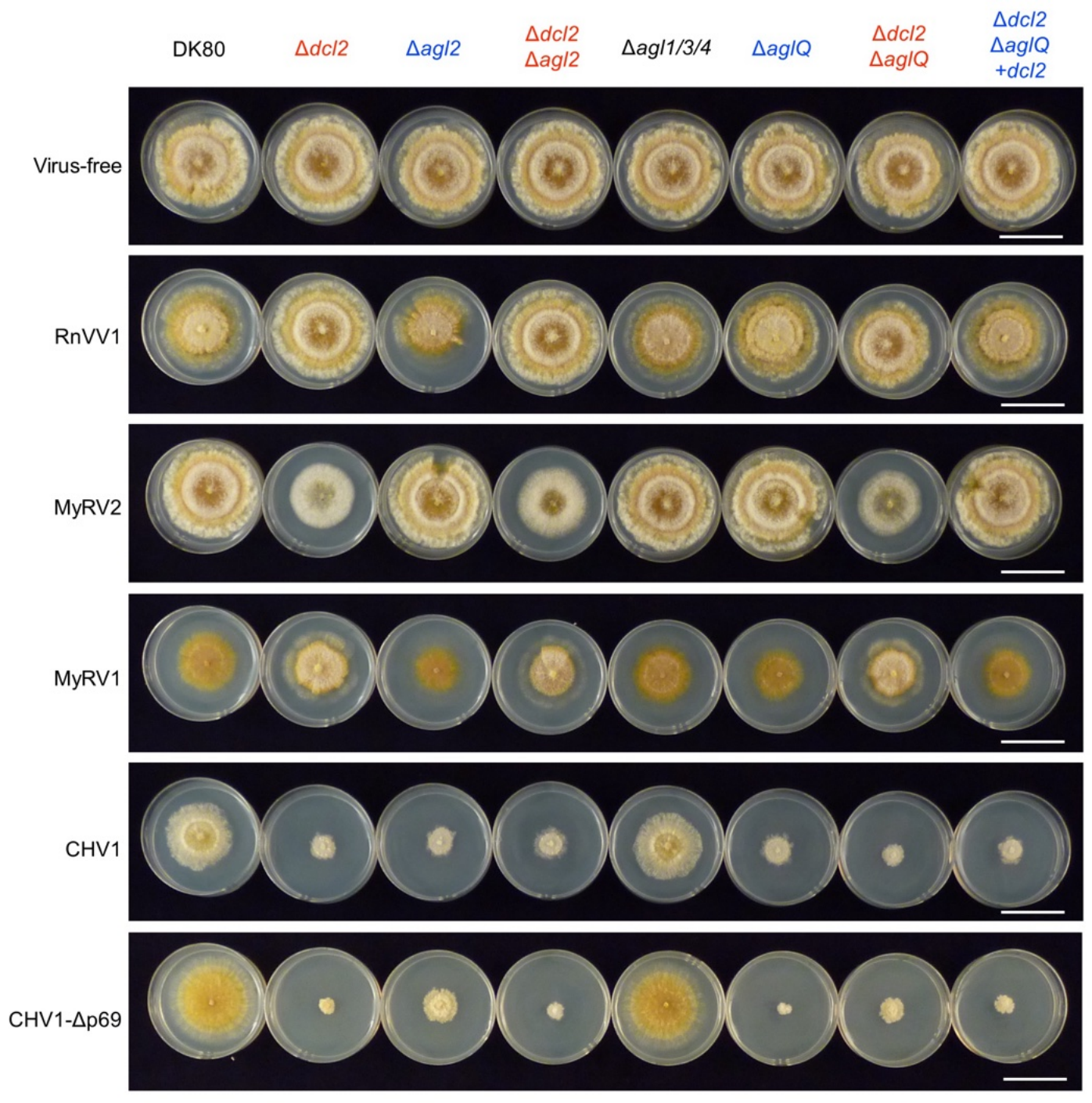
DK80
Δdcl2
Δagl2
Δdcl2 Δagl2
Δagl1/3/4
ΔaglQ
Δdcl2 ΔaglQ
Δdcl2 ΔaglQ +dcl2
Virus-free
RnVV1
MyRV2
MyRV1
CHV1
CHV1-Δp69

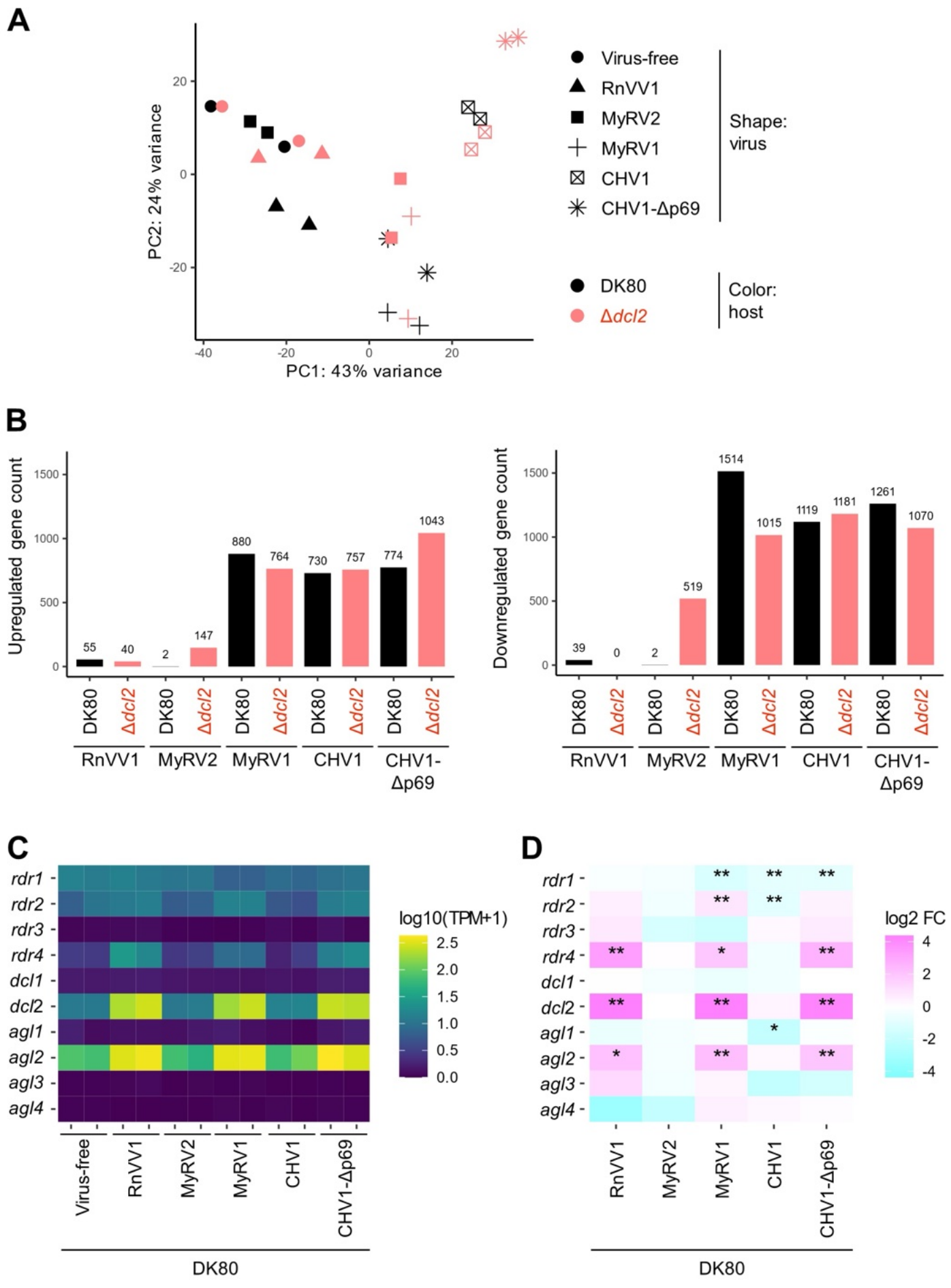
A
PC2: 24% variance
PC1: 43% variance
Virus-free
RnVV1
MyRV2
MyRV1
CHV1
CHV1-Δp69
Shape: virus
DK80
Δdcl2
Color: host
B
Upregulated gene count
55
40
2
147
880
764
730
757
774
1043
Downregulated gene count
39
0
2
519
1514
1015
1119
1181
1261
1070
DK80
Δdcl2
RnVV1
MyRV2
MyRV1
CHV1
CHV1-Δp69
C
rdr1
rdr2
rdr3
rdr4
dcl1
dcl2
agl1
agl2
agl3
agl4
log10(TPM+1)
Virus-free
RnVV1
MyRV2
MyRV1
CHV1
CHV1-Δp69
DK80
D
log2 FC
DK80

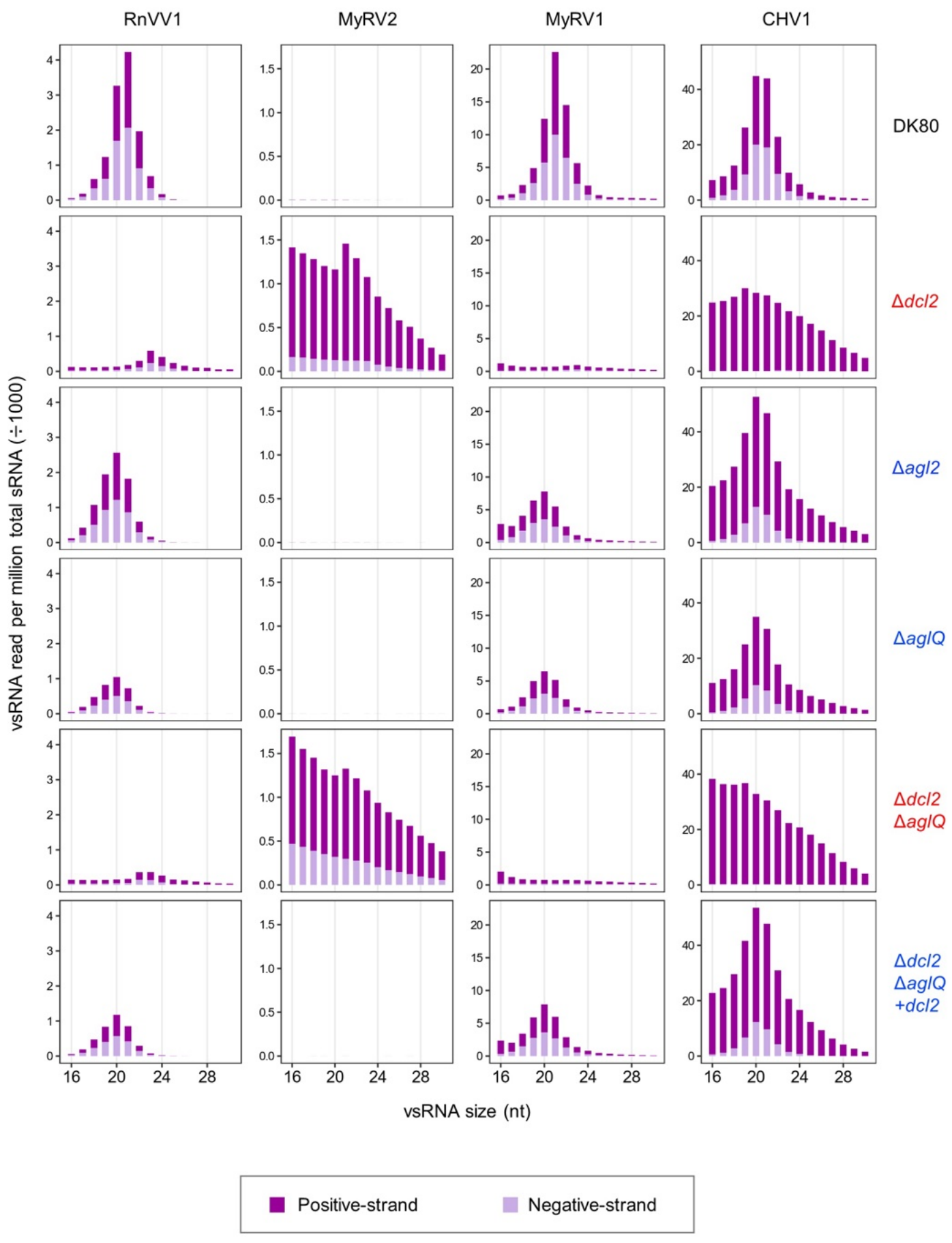
RnVV1
MyRV2
MyRV1
CHV1
DK80
Δdcl2
Δagl2
ΔaglQ
Δdcl2
ΔaglQ
Δdcl2
ΔaglQ
+dcl2
vsRNA read per million total sRNA (÷1000)
vsRNA size (nt)
Positive-strand
Negative-strand

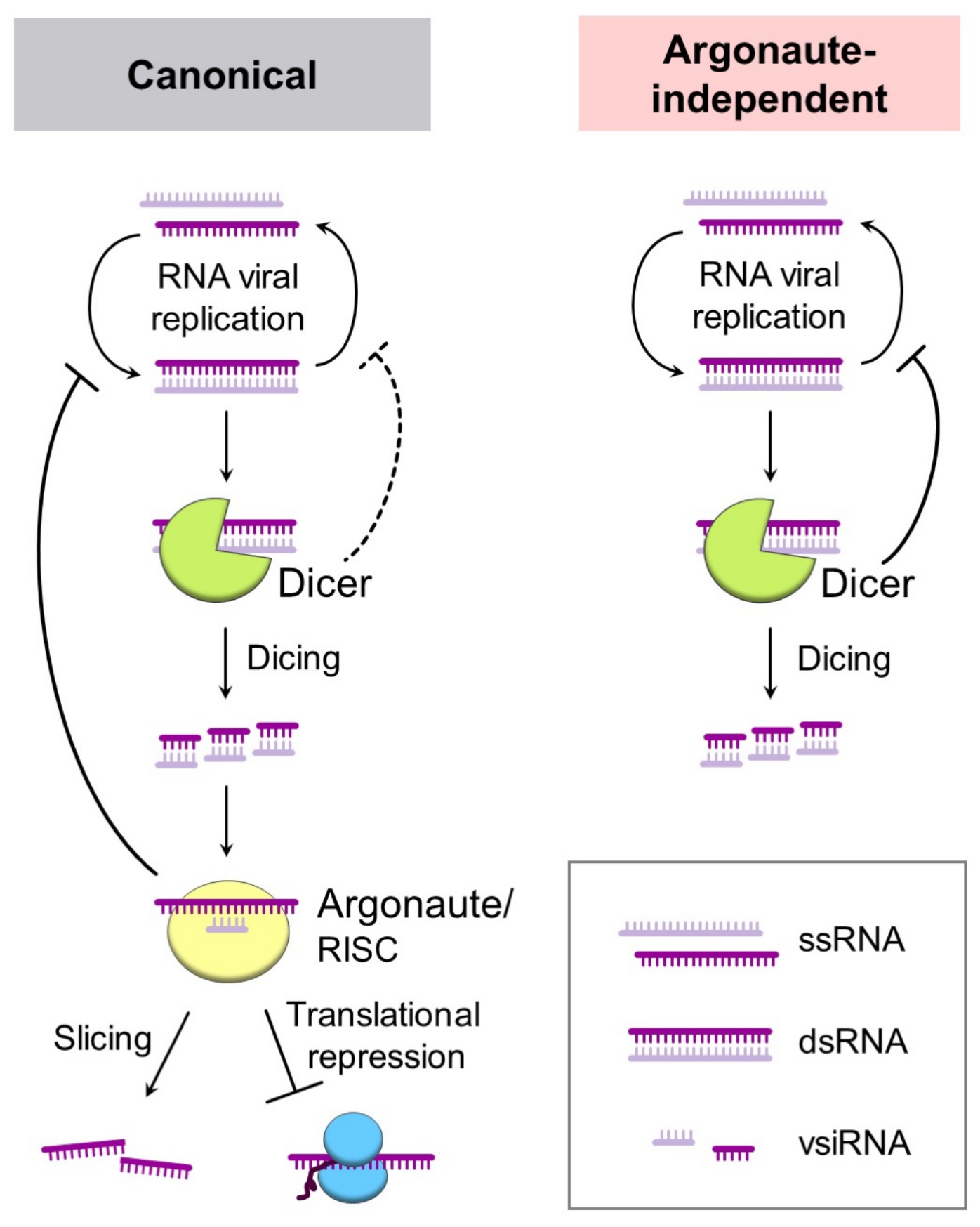
Canonical
Argonaute-independent
RNA viral replication
Dicer
Dicing
Argonaute/ RISC
Slicing
Translational repression
RNA viral replication
Dicer
Dicing
ssRNA
dsRNA
vsiRNA

Supplementary Information for

Argonaute-independent, Dicer-dependent antiviral defense against RNA viruses

Yukiyo Sato[a, *], Hideki Kondo[a], and Nobuhiro Suzuki[a, 1]

[a]Institute of Plant Science and Resources, Okayama University, Kurashiki, Okayama 710-0046, Japan

[1] To whom correspondence may be addressed. Corresponding Author: Dr. Nobuhiro Suzuki
ORCID ID, http://orcid.org/0000-0003-0097-9856
Agrivirology Laboratory
Institute of Plant Science and Resources
Okayama University
Kurashiki, Okayama 710-0046, Japan
Tel. 81(86) 434-1230
Fax. 81(86) 434-1232
e-mail. nsuzuki@okayama-u.ac.jp

*Present Address: Institute for Plant Sciences, University of Cologne, Cologne, Germany

Short title: AGO-independent, Dicer-independent antiviral defense

Data information:

Supplemental Materials and Methods with 36 references

Supplemental figures, 8.

Supplemental tables, 4.

SI Materials and Methods

Search for Argonaute domains

AGL1, AGL2, AGL3, and AGL4 (GenBank accessions: ACY36939.1, ACY36940.1, ACY36941.1, and ACY36942.1, respectively) are encoded by *agl1*, *agl2*, *agl3*, and *agl4*, respectively. The database Pfam 35.0 database (1) was searched for the conserved domain with these AGL amino acid sequences by hmmscan in HMMER version 3.3.2 (e-value < 0.001) (https://www.mankier.com/package/hmmer) (2). The domain positions were mapped by using ggplot2 version 3.4.2 (https://ggplot2.tidyverse.org/).

Vector construction

All vectors were constructed with In-Fusion HD Cloning kit (TaKaRa Bio). The polymerase chain reaction (PCR) insert was prepared with primers and template listed in *SI Appendix*, Table S1 by KOD -Plus- Neo (TOYOBO) (or PrimerSTAR GXL DNA polymerase [TaKaRa Bio] for one construct; see below) according to the manufacturer's instructions. The vectors were linearized with restriction enzymes provided by New England Biolabs, TOYOBO, or TaKaRa Bio, according to the manufacturer's instructions.

For fungal gene disruption, three backbone vectors for homologous recombination (HR) were generated—pGEM::loxPneoR, pGEM::loxPhygRinv, and pGEM::loxPntcRinv—which contain the antibiotic resistance gene as a selectable marker gene (SMG) cassette against neomycin, hygromycin, or nourseothricin (NTC), respectively, and a *loxP* sequence at both ends. For pGEM::loxPneoR, the neomycin resistance gene cassette (*neoR*) (3) was amplified from pCPXNeo (4), with primers that contain the *loxP* sequence. The amplified *neoR* was cloned into the *Eco*RI sites of the pGEM-T Easy vector (Promega). For pGEM::loxPhygRinv, the hygromycin-resistance gene cassette (*hygR*) was amplified from pCPXHY3 (5). The *hygR* amplicon was replaced by *neoR* in the pGEM::loxPneoR linearized at the two *Eco*RI sites and placed between *neoR* and *loxP* at both ends. Because the *loxP* sequence is repeated, the cloning reaction can produce two types of products, with *hygR* in the same or inverse orientation compared to the orientation of *neoR* in pGEM::loxPneoR. The latter one (inverse orientation) was used; thus, "inv" was added to the vector name. For pGEM::loxPntcRinv, the NTC resistance gene cassette (*ntcR*) was amplified from pAL12-Lifeact (6). Then, the *ntcR* amplicon was then was replaced for the promoter and coding sequence of *hygR* in pGEM::loxPhygRinv linearized with *Eco*RI and *Bam*HI.

To construct vectors for disruption of the target genes, approximately 0.75 kilobase pair (kbp) upstream and downstream flanking regions (5′ and 3′ arms, respectively) of the target genes were respectively cloned into the *Sph*I and *Sal*I sites, respectively, of the HR backbone vectors. The homology arm sequences were obtained from the *Cryphonectria parasitica* EP155 v2.0 database (https://mycocosm.jgi.doe.gov/Crypa2) provided by the Joint Genome Institute (JGI). The homology arms for *dcl1* and *dcl2* were cloned into pGEM::loxPhygRinv. The homology arms for *agl1*, *agl2*, *agl3*,

and *agl4* were cloned into pGEM::loxPneoR, pGEM::loxPhygRinv, and/or pGEM::loxPntcRinv for multiple gene disruption (*SI Appendix*, Figs. S1 and S2*A*). For cloning into the pGEM::loxPneoR vector that contains the *Sph*I site in *neoR*, the 5′ and 3′ arms were first sub-cloned into the *Sph*I and *Sal*I sites of the pGEM-T Easy backbone without *neoR*. Then, the sub-cloning vectors were linearized with *Eco*RI and connected with the *neoR* (P_{gpd}-*nptII*-T_{tub}) amplicon.

The plasmid vector termed pCPXHY3::Cre was generated to introduce Cre recombinase into *C. parasitica*. The Cre coding sequence (CDS) was amplified from pKAES175 (7) and cloned into the *Not*I and *Sph*I sites of pCPXHY3.

The plasmid vector termed pNeo3::P_{dcl2}-*dcl2* was generated for genetic complementation of *dcl2*. Prior to cloning, the backbone vectors pXYLHY3 and pXYLNeo3 were generated for use in other studies. pXYLHY3 has a xylose-responsive promoter (P_{xyl}) from *Colletotrichum orbiculare*, while pCPXHY3 has a constitutive expression promoter (P_{gpd}) from *C. parasitica*. The promoter P_{xyl} was amplified from pCB1636_lox_HPT-TK (8) using a primer with the *Spe*I and *Xho*I sequences to enable replacement of P_{xyl} with any other promoter. Then, the P_{xyl} amplicon was then cloned into the *Xcm*I and *Hind*III sites of pCPXHY3 to replace P_{gpd}. pXYLNeo3 was generated by replacing *hygR* in pXYLHY3 with *neoR*. For the replacement, *neoR* was amplified from the pCRPNeo vector. Then, the *neoR* amplicon was cloned into pXYLHY3 linearized with *Eco*RI and *Xba*I to replace *hygR*. The vector pNeo3::P_{dcl2}-*dcl2* was generated by replacing P_{xyl} in pXYLNeo3 with the *dcl2* gene with its native promoter (2000 bp upstream of the start codon, the region transcriptionally responsive to viral infection (9)) (P_{dcl2}-*dcl2*). For the replacement, P_{dcl2}-*dcl2* was amplified from the genomic DNA of *C. parasitica* EP155 by PrimerSTAR GXL DNA polymerase (TaKaRa Bio) and cloned into the *Xho*I and *Sph*I sites of pXYLNeo3.

Fungal transformation

Spheroplasts of *C. parasitica* were prepared as described previously (10), with minor modifications to the original protocol (11). For gene disruption, each HR cassette was amplified from the plasmid vector described above by using the forward primer for the 5′ arm and the reverse primer for the 3′ arm (*SI Appendix*, Table S1) by KOD -Plus- Neo (TOYOBO). The amplicon was purified with Wizard SV Gel and PCR Clean-Up System (Promega). The purified amplicon (5 μg) was introduced into the fungal spheroplasts (1–2 × 10^7 cells/mL × 100 μL) by a method mediated by a polyethylene glycol (PEG)-mediated method, as described previously (11). Single colonies harboring *neoR*, *hygR*, or *ntcR* were selected with 20 μg/mL G418 sulfate, 40 μg/mL hygromycin B, or 20 μg/mL NTC, respectively, in 1% top agar layered on regeneration medium containing regenerated spheroplasts. The single colonies on the top agar were further selected on PDA containing each antibiotic at the same final concentration. Among the antibiotic-resistant colonies on PDA, the deletion mutants were screened by direct colony PCR with Quick Taq HS DyeMix (TOYOBO). The screening was performed with combinations of a forward primer targeting the upstream region outside the 5′ arm on the fungal genome

and a reverse primer targeting the SMG. The screened mutants were further cultured on PDA with antibiotic under sunlight to induce conidiation. Single conidia (monokaryotic) were isolated on new antibiotic PDA to remove wild type karyotypes. The complete deletion of the target genes was further validated by PCR and southern blotting as described below.

For single to triple gene disruption, three different SMGs (*neoR*, *hygR*, and *ntcR*) were utilized, as summarized in *SI Appendix*, Fig. S2*A*. To generate Δ*dcl1* and Δ*dcl2*, *dcl1* and *dcl2* were replaced with *hygR* in the DK80 background. To generate Δ*agl1* to Δ*agl4*, *agl1* to *agl4* were replaced with *neoR* in the DK80 background. To generate the double mutant Δ*dcl2*Δ*agl2*, *agl2* was replaced with *neoR* in the Δ*dcl2* background. To generate the triple mutant Δ*agl1/3/4*, *agl4* was first replaced with *hygR* in the Δ*agl1* background, and then *agl3* was replaced with *ntcR*.

For quadruple and quintuple gene disruption, the SMGs were removed by the Cre-*loxP* system (12). First, the *C. parasitica* transformants that produce functional Cre recombinase were generated (*SI Appendix*, Figs. S2*B* and S2*C*). Δ*agl4* (*agl4* disruptant with *neoR*) was transformed with pCPXHY3::Cre by the PEG-mediated method described above (for plasmid, 10 μg was used for each transformation instead of 5 μg PCR amplicon). This transformant is termed Δ*agl4*+*Cre*. The transformants were selected based on hygromycin resistance, genotyping, and Cre activity. The Cre activity was estimated by PCR targeting an upstream region of the 5′ arm to the end of the 3′ arm of *agl4* (*SI Appendix*, Fig. S2*B* and Table S2). The transformant showing complete excision of *neoR* (Δ*agl4*+*Cre* #10) (*SI Appendix*, Fig. S2*C*) was selected as a Cre donor for the following anastomosis-mediated SMG excision (12) (*SI Appendix*, Fig. S2*D*). Briefly, the Cre donor (hygromycin resistant) was cultured alongside Δ*agl1/3/4*, which is resistant to all three antibiotics (neomycin, hygromycin, and NTC) for horizontal transfer of Cre recombinase via hyphal anastomosis. After co-culturing for 2 weeks, a small (1 mm^3) mycelial plug was taken from the Cre recipient side adjacent to the contact zone at the colony periphery. The mycelial plug was transferred to PDA without antibiotics and grown under sunlight to induce conidiation. The generated conidia were suspended in sterile water and spread on fresh antibiotic-free PDA for isolation. The single conidial sub-isolates were transferred to PDA supplemented with 50 μg/mL hygromycin to screen for the gene disruptants that lost *hygR* and to exclude the hygromycin resistant Cre donor that is resistant to hygromycin. The screening yielded a Δ*agl1/3/4* strain that lost *hygR* but kept *neoR* and *ntcR*. This Δ*agl1/3/4* strain was used for the analyses in this study. Then, Δ*aglQ* was generated by replacing *agl2* with *hygR* in this Δ*agl1/3/4* background. The SMGs in Δ*aglQ* were removed by the same Cre-*loxP* system (*SI Appendix*, Fig. S2*D*). The Δ*aglQ* strain, which lost *hygR* and *neoR* but kept *ntcR* was obtained and used for the analyses in this study. For the SMG removal experiments, approximately 100–500 independent conidial sub-isolates were screened. Then, Δ*dcl2*Δ*aglQ* was generated by replacing *dcl2* with *hygR* in the Δ*aglQ* background.

The *dcl2* complementation strain was generated in Δ*dcl2*Δ*aglQ*, namely Δ*dcl2*Δ*aglQ*+*dcl2*, by transforming Δ*dcl2*Δ*aglQ* with pNeo3::P_{dcl2}-*dcl2* by the PEG-mediated method as described above. The transformants were selected for the neomycin resistance, genotype, and the DK80-like tolerance to

RnVV1.

Virus inoculation

Virus-free strains were inoculated with viruses mainly via hyphal fusion/anastomosis (Fig. 2*A*) (13). A small mycelial plug (≈1 mm^3) from each virus donor fungal strain and each virus-free recipient fungal strain (Table 1 and *SI Appendix*, Table S3) was placed onto a central part on PDA (9 cm in diameter) with a distance of around 5 mm^3 between the donor and the recipient. The donor and recipient were cultured for approximately 1 week to allow hyphal anastomosis between the two fungal strains and consequent horizontal virus transfer to the recipient side. After the dual culture, a small mycelial plug (≈1 mm^3) was excised from the recipient side at the farthest part from the donor and recipient hyphal contact. The excised mycelial plugs were transferred to new PDA and sub-cultured for a few days for further analyses. For CHV1 and CHV1-Δp69, which severely inhibit recipient hyphal elongation and may induce contamination by donor hyphae, recipient colonies were repeatedly fused with the virus-free recipients.

For one experiment (Fig. 2*E*), RnVV1 was inoculated by virion transfection (Fig. 2*D*) (14). Crude virus particles of RnVV1 were extracted from *C. parasitica* EP155Δ*dcl2*/RnVV1 (15), as described previously (16), by omitting the sucrose gradient fractionation and the following procedures. The crude virus particles were purified by filtration through a 0.22 μm pore size filter (Millipore) by centrifugation. The flow-throw was used to transfect spheroplasts of DK80, Δ*dcl2*, and Δ*agl2*, as described previously (10), by omitting the hygromycin selection step. Virus-infected colonies were screened by direct colony reverse transcription–polymerase chain reaction (RT-PCR) (17) with the Prime Script One Step RT-PCR Kit, Ver.2 (Dye Plus), as described previously (18).

PCR genotyping and Southern blotting

Genomic DNA was extracted from fungal mycelia cultured on PDA-cellophane for 2 or 3 days. Briefly, the mycelia were ground with a mortar and pestle in liquid nitrogen. The frozen mycelial powder was mixed with a 10-fold volume (per fresh mycelial weight) of a nucleic acid extraction buffer (50 mM NaCl, 100 mM Tris-HCl [pH 8.0], 10 mM ethylenediaminetetraacetic acid [EDTA, pH 8.0], and 0.5% sodium dodecyl sulfate [SDS]). Total nucleic acids were extracted with phenol/chloroform/isoamyl alcohol (PCIA, prepared with phenol saturated with TE buffer [pH 7.9]) followed by chloroform/isoamyl alcohol (CIA) extraction. The crude total nucleic acids were treated with 10 μg/mL RNase A (Sigma-Aldrich Co., LLC) at 37°C for 30 min, purified by PCIA and CIA extraction followed by 2-propanol precipitation and rinsing with 70% (v/v) ethanol, and resuspended in TE buffer. The concentration of the purified DNA was measured with a NanoDrop spectrophotometer.

PCR genotyping was carried out in 10 μL of Quick Taq HS DyeMix (Toyobo, Co. Ltd.) with 10 ng of purified genomic DNA and primers listed in *SI Appendix*, Table S2 according to the manufacturer's instructions (three-step cycle). PCR products were electrophoresed in 1.0% (w/v) agarose gel in 0.5×

TAE and stained with ethidium bromide (EtBr). For all gel electrophoresis, the size of the PCR products was checked with GeneRuler 1 kb DNA Ladder (Thermo Scientific).

For Southern blotting, 8–10 µg (constant amount for each gel) of genomic DNA was digested with restriction enzymes (New England Biolabs or TOYOBO) overnight at the temperature recommended by the manufacturers. The *dcl1* and *dcl2* loci were analyzed with *Bam*HI; the *agl1*, *agl2*, and *agl4* loci with *Pst*I; and the *agl3* locus with *Xho*I (*SI Appendix*, Fig. S1). The digested DNA was purified by PCIA extraction followed by ethanol precipitation. All recovered purified DNA fragments were electrophoresed in a 1.0% (w/v) agarose gel with 0.5× TAE at constant 100 V. The electrophoresed DNA on the gel was blotted onto a nylon membrane Hybond-N+ (GE Healthcare) according to the manufacturer's instructions. Briefly, the gel was depurinated in 0.125 M HCl for 10 minutes with gentle agitation. The gel was then incubated in denaturation buffer (1.5 M NaCl and 0.5 N NaOH) for 30 min with gentle agitation, followed by incubation in neutralization buffer (1.5 M NaCl and 0.5 M Tris-HCl, pH 7.5) for 30 min with gentle agitation. Denatured DNA on the gel was transferred to Hybond-N+ by capillary blotting using filter papers immersed in 20× SSC (0.3 M trisodium citrate and 3 M NaCl). After overnight, the transferred DNA was crosslinked to the membrane by UVP Crosslinker CL-1000 at 240,000 µJ/cm^2. The target genomic region on the membrane was detected according to the DIG (digoxigenin) Application Manual provided by Roche Applied Science (https://www.sigmaaldrich.com/deepweb/assets/sigmaaldrich/marketing/global/documents/199/985/dig-application-manual-for-filter-hybridisation-iris.pdf). DIG-labeled DNA probes were synthesized with the PCR DIG Labeling Mix (Roche), the primers listed in *SI Appendix*, Table S1 (primer sets for *dcl1*-5′arm, *dcl2*-5′arm, *agl1*-5′arm, *agl2*-3′arm, *agl3*-5′arm, or *agl4*-5′arm for the respective loci), and plasmid templates containing the target genomic regions. Chemiluminescence was detected with the ImageQuant LAS 4000 (GE Healthcare).

RNA extraction, northern blotting, and RT-PCR

RNA was extracted from fungal mycelia cultured on PDA-cellophane for 3 days. Briefly, the frozen mycelial powder was mixed with a 10-fold volume (per mycelial fresh weight) of the nucleic acid extraction buffer described above and subjected to PCIA (prepared with phenol saturated with water) extraction, CIA extraction, and ethanol precipitation. The total nucleic acid pellets were rinsed with 70% ethanol, dried, and dissolved in sterile Milli-Q water. The total RNA fraction consisting of both dsRNA and ssRNA was purified by treating total nucleic acids with RQ1 RNase-Free DNase (Promega) at 37°C for 30 min followed by phenol-chloroform extraction, PCIA extraction, CIA extraction, ethanol precipitation, and rinsing with 70% ethanol, and then dissolved in sterile Milli-Q water. The RNA concentration was measured using the NanoDrop spectrophotometer. The total RNA fraction was used for northern blotting (Fig. 3*A–E*), RT-PCR (*SI Appendix*, Fig. S6), and small RNA-Seq. The ssRNA-enriched fraction was precipitated from the total nucleic acids with lithium chloride (LiCl, final concentration 2 M, which is supposed to enrich high molecular-weight ssRNA (19)), rinsed with 70%

ethanol, and dissolved in sterile Milli-Q water. The crude ssRNA-enriched fraction was used for northern blotting and RT-PCR (Figs. 2 and 3*F* and *G*, and *SI Appendix*, Figs. S5 and S7). The ssRNA-enriched fraction was further purified by treatment with RQ1 RNase-Free DNase followed by DNase purification as described above. The DNase-purified ssRNA-enriched fraction was used for RNA-Seq.

Northern blotting was performed with two different methods for the total RNA and ssRNA-enriched fractions. The total RNA fraction (5 μg per lane) was electrophoresed on a 1% agarose gel in 0.5× TAE and stained with EtBr after electrophoresis. The total RNA in the gel was denatured by alkaline treatment after electrophoresis and blotted onto a nylon membrane (Hybond-N+, GE Healthcare), as described previously (20). The ssRNA-enriched fraction (2 μg per lane for viral detection or 10 μg per lane for host mRNA and some RnVV1/MyRV2 detections; constant for each gel) was pre-stained with EtBr, denatured during electrophoresis in MOPS-formaldehyde gel, and blotted onto Hybond-N+ immediately after the electrophoresis, as described previously (21). Target RNA bands on the membranes were detected by using complementary DNA (cDNA) probes labeled with DIG by the PCR DIG Labeling Mix (Roche). Primers used for the cDNA probe preparation are listed in *SI Appendix*, Table S2. Plasmids (pGEM-T or pCPXHY3 backbone) containing cDNA of the target viral or host mRNA regions were used as templates.

Quantitative reverse transcription-polymerase chain reaction (qRT-PCR) was performed with ReverTra Ace qPCR RT Kit (TOYOBO) and THUNDERBIRD SYBR qPCR Mix (TOYOBO) according to manufacturer's instructions. Primers used for qRT-PCR are listed in *SI Appendix*, Table S2. The real-time PCR was performed in qTOWER3/G (Analytik Jena). The relative viral RNA level was calculated by the $2^{-\Delta\Delta CT}$ method with the host actin gene as internal control and DK80-infected with the respective viruses as a calibrator (22).

Semi-qRT-PCR was performed with Prime Script One Step RT-PCR Kit, Ver.2 (Dye Plus) (TaKaRa Bio) in a volume of 10 μL using 10 μg of purified total RNA or ssRNA-enriched fraction as a template with the primers listed in *SI Appendix*, Table S2. The standard three-step PCR was carried out according to the manufacturer's instructions. The PCR products were electrophoresed in 1.0% (w/v) agarose gel in 0.5× TAE and stained with EtBr. The relative band intensity was quantified with ImageJ 1.5.3t (https://imagej.nih.gov/ij/).

RNA-Seq and small RNA-Seq analyses

The RNA-Seq library was constructed with the KAPA mRNA Capture kit (Kapa Biosystems, #KK8440) and the MGIEasy RNA Directional Library Prep set (MGI, #1000006385) by GenomeRead Inc. The cDNA library was sequenced at a 17 million read depth of 2 × 150 bp paired-end by DNBSEQ-G400RS (MGI) by GenomeRead Inc. The RNA-Seq reads were subjected to quality control and adaptor trimming by fastp version 0.19.5 (23). The trimmed RNA-Seq reads were mapped to the masked genome sequence of *C. parasitica* strain EP155 (Cryphonectria_parasiticav2.nuclearAssembly.masked) (24) by HISAT2 version 2.2.1 (25). The output SAM files were converted into BAM files, sorted, and indexed by

SAMtools version 1.7 (26). The reads mapped to respective genes in a gene catalog (Cparasiticav2.GeneCatalog20091217.gff) (24) were counted by htseq-count version 2.0.2 with the options -f bam, -r pos, -i name, and -s reverse (27). Differentially expressed genes (DEGs) were analyzed by DESeq2 version 1.42.0 (28) with a minimum read threshold of one. Transcripts per million (TPM) were calculated according to the formula described previously (29). The DEG analysis results were visualized with ggplot2 version 3.4.3 (https://ggplot2.tidyverse.org/).

For small RNA-Seq analysis, total RNA extracted from virus-infected *C. parasitica* strains was sent to Macrogen Inc. The small RNA cDNA library was constructed using the NEBNext Small RNA Library Prep Set for Illumina (New England Biolabs) and subsequently sequenced in a single read (SE) (1 × 50 nt) run on the Illumina HiSeq 2500 platform. The adapter was trimmed from the raw reads (25~64 million reads); then, the reads were filtered for a size range of 16–32 nt using CLC Genomic Workbench (version 22; CLC Bio-Qiagen, Aarhus, Denmark). The retained reads in each library were then mapped to respective virus genome or genomic segments using the Read Mapping algorithm in the CLC Genomics Workbench. The virus-derived small RNA reads were used for further analysis with the MISIS-2 program (30).

SI REFERENCES

1. T. Paysan-Lafosse *et al.*, InterPro in 2022. *Nucleic Acids Res* **51**, D418-D427. (2023).
2. S. R. Eddy, Accelerated Profile HMM Searches. *PloS Comput Biol* **7**, e1002195. (2011).
3. Q. Sun, G. H. Choi, D. L. Nuss, Hypovirus-responsive transcription factor gene *pro1* of the chestnut blight fungus *Cryphonectria parasitica* is required for female fertility, asexual spore development and stable maintenance of hypovirus infection. *Eukaryot Cell* **8**, 262-270 (2009).
4. Q. Sun, G. H. Choi, D. L. Nuss, A single Argonaute gene is required for induction of RNA silencing antiviral defense and promotes viral RNA recombination. *Proc Natl Acad Sci U S A* **106**, 17927-17932 (2009).
5. L. H. Guo, L. Sun, S. Chiba, H. Araki, N. Suzuki, Coupled termination/reinitiation for translation of the downstream open reading frame B of the prototypic hypovirus CHV1-EP713. *Nucleic Acids Res* **37**, 3645-3659 (2009).
6. A. Lichius, N. D. Read, A versatile set of Lifeact-RFP expression plasmids for live-cell imaging of F-actin in filamentous fungi. *Fungal Genetics Reports* **57**, Article 4. https://doi.org/10.4148/1941-4765.1070 (2010).
7. S. Florea, K. Andreeva, C. Machado, P. M. Mirabito, C. L. Schardl, Elimination of marker genes from transformed filamentous fungi by unselected transient transfection with a Cre-expressing plasmid. *Fungal Genet Biol* **46**, 721-730 (2009).
8. K. Yamada, T. Yamamoto, K. Uwasa, K. Osakabe, Y. Takano, The establishment of multiple knockout mutants of *Colletotrichum orbiculare* by CRISPR-Cas9 and Cre-*loxP* systems. *Fungal Genet Biol* **165**, 103777 (2023).
9. I. B. Andika, A. Jamal, H. Kondo, N. Suzuki, SAGA complex mediates the transcriptional up-regulation of antiviral RNA silencing. *Proc Natl Acad Sci U S A* **114**, E3499-E3506 (2017).
10. Y. Sato, S. Hisano, N. Suzuki, Exploration of the yadokari/yadonushi nature of YkV3 and RnMBV3 in the original host and a model filamentous fungus. *Virus Res* **334**, 199155 (2023).
11. A. C. L. Churchill, L. M. Ciuffetti, D. R. Hansen, H. D. Vanetten, N. K. Van Alfen, Transformation of the fungal pathogen *Cryphonectria parasitica* with a variety of heterologous plasmids. *Current Genetics* **17**, 25-31 (1990).
12. D. X. Zhang, H. L. Lu, X. Liao, R. J. St Leger, D. L. Nuss, Simple and efficient recycling of fungal selectable marker genes with the Cre-*loxP* recombination system via anastomosis. *Fungal Genet Biol* **61**, 1-8 (2013).
13. N. K. Van Alfen, R. A. Jaynes, S. L. Anagnostakis, P. R. Day, Chestnut Blight: Biological Control

by Transmissible Hypovirulence in *Endothia parasitica*. *Science* **189**, 890-891 (1975).
14. B. I. Hillman, S. Supyani, H. Kondo, N. Suzuki, A reovirus of the fungus *Cryphonectria parasitica* that is infectious as particles and related to the *Coltivirus* genus of animal pathogens. *J Virol* **78**, 892-898 (2004).
15. S. Chiba, Y. H. Lin, H. Kondo, S. Kanematsu, N. Suzuki, A novel victorivirus from a phytopathogenic fungus, *Rosellinia necatrix* is infectious as particles and targeted by RNA silencing. *J Virol* **87**, 6727-6738 (2013).
16. S. Chiba *et al.*, A novel bipartite double-stranded RNA mycovirus from the white root rot fungus *Rosellinia necatrix*: molecular and biological characterization, taxonomic considerations, and potential for biological control. *J Virol* **83**, 12801-12812 (2009).
17. S. Urayama *et al.*, Rapid detection of Magnaporthe oryzae chrysovirus 1-A from fungal colonies on agar plates and lesions of rice blast. *J Gen Plant Pathol* **81**, 97-102 (2015).
18. Y. Sato *et al.*, Hadaka virus 1: a capsidless eleven-segmented positive-sense single-stranded RNA virus from a phytopathogenic fungus, *Fusarium oxysporum*. *mBio* **11**, e00450-00420. (2020).
19. J. R. Diaz-Ruiz, J. M. Kaper, Isolation of viral double-stranded RNAs using a LiCl fractionation procedure. *Prep Biochem* **8**, 1-17 (1978).
20. Y. Sato, S. Hisano, C. J. Lopez-Herrera, H. Kondo, N. Suzuki, Three-layered complex interactions among capsidless (+)ssRNA yadokariviruses, dsRNA viruses, and a fungus. *mBio* **13**, e0168522 (2022).
21. Y. Sato *et al.*, A new tetra-segmented splipalmivirus with divided RdRP domains from *Cryphonectria naterciae*, a fungus found on chestnut and cork oak trees in Europe. *Virus Res* **307**, 198606. (2022).
22. K. J. Livak, T. D. Schmittgen, Analysis of relative gene expression data using real-time quantitative PCR and the 2(-Delta Delta C(T)) method. *Methods* **25**, 402-408 (2001).
23. S. Chen, Y. Zhou, Y. Chen, J. Gu, fastp: an ultra-fast all-in-one FASTQ preprocessor. *Bioinformatics* **34**, i884-i890 (2018).
24. J. A. Crouch *et al.*, Genome sequence of the chestnut blight fungus *Cryphonectria parasitica* EP155: A fundamental resource for an archetypical invasive plant pathogen. *Phytopathology* **110**, 1180-1188. (2020).
25. D. Kim, J. M. Paggi, C. Park, C. Bennett, S. L. Salzberg, Graph-based genome alignment and genotyping with HISAT2 and HISAT-genotype. *Nat Biotechnol* **37**, 907-915 (2019).
26. P. Danecek *et al.*, Twelve years of SAMtools and BCFtools. *Gigascience* **10** (2021).
27. S. Anders, P. T. Pyl, W. Huber, HTSeq--a Python framework to work with high-throughput sequencing data. *Bioinformatics* **31**, 166-169 (2015).
28. M. I. Love, W. Huber, S. Anders, Moderated estimation of fold change and dispersion for RNA-seq data with DESeq2. *Genome Biol* **15**, 550 (2014).
29. B. Li, V. Ruotti, R. M. Stewart, J. A. Thomson, C. N. Dewey, RNA-Seq gene expression estimation with read mapping uncertainty. *Bioinformatics* **26**, 493-500 (2010).
30. J. Seguin, P. Otten, L. Baerlocher, L. Farinelli, M. M. Pooggin, MISIS-2: A bioinformatics tool for in-depth analysis of small RNAs and representation of consensus master genome in viral quasispecies. *J Virol Methods* **233**, 37-40 (2016).
31. B. I. Hillman, B. T. Halpern, M. P. Brown, A viral dsRNA element of the chestnut blight fungus with a distinct genetic organization. *Virology* **201**, 241-250 (1994).
32. C. D. Smart *et al.*, Cryphonectria hypovirus 3, a virus species in the family hypoviridae with a single open reading frame. *Virology* **265**, 66-73 (1999).
33. A. Aulia, I. B. Andika, H. Kondo, B. I. Hillman, N. Suzuki, A symptomless hypovirus, CHV4, facilitates stable infection of the chestnut blight fungus by a coinfecting reovirus likely through suppression of antiviral RNA silencing. *Virology* **533**, 99-107 (2019).
34. A. Aulia, M. Tabara, P. Telengech, T. Fukuhara, N. Suzuki, Dicer monitoring in a model filamentous fungus host, *Cryphonectria parasitica*. *Curr Res Virol Sci* **1**, 100001. (2020).
35. D. X. Zhang, M. J. Spiering, D. L. Nuss, Characterizing the roles of *Cryphonectria parasitica* RNA-dependent RNA polymerase-like genes in antiviral defense, viral recombination and transposon transcript accumulation. *PLoS One* **9**, e108653 (2014).
36. G. C. Segers, X. Zhang, F. Deng, Q. Sun, D. L. Nuss, Evidence that RNA silencing functions as an antiviral defense mechanism in fungi. *Proc Natl Acad Sci U S A* **104**, 12902-12906 (2007).

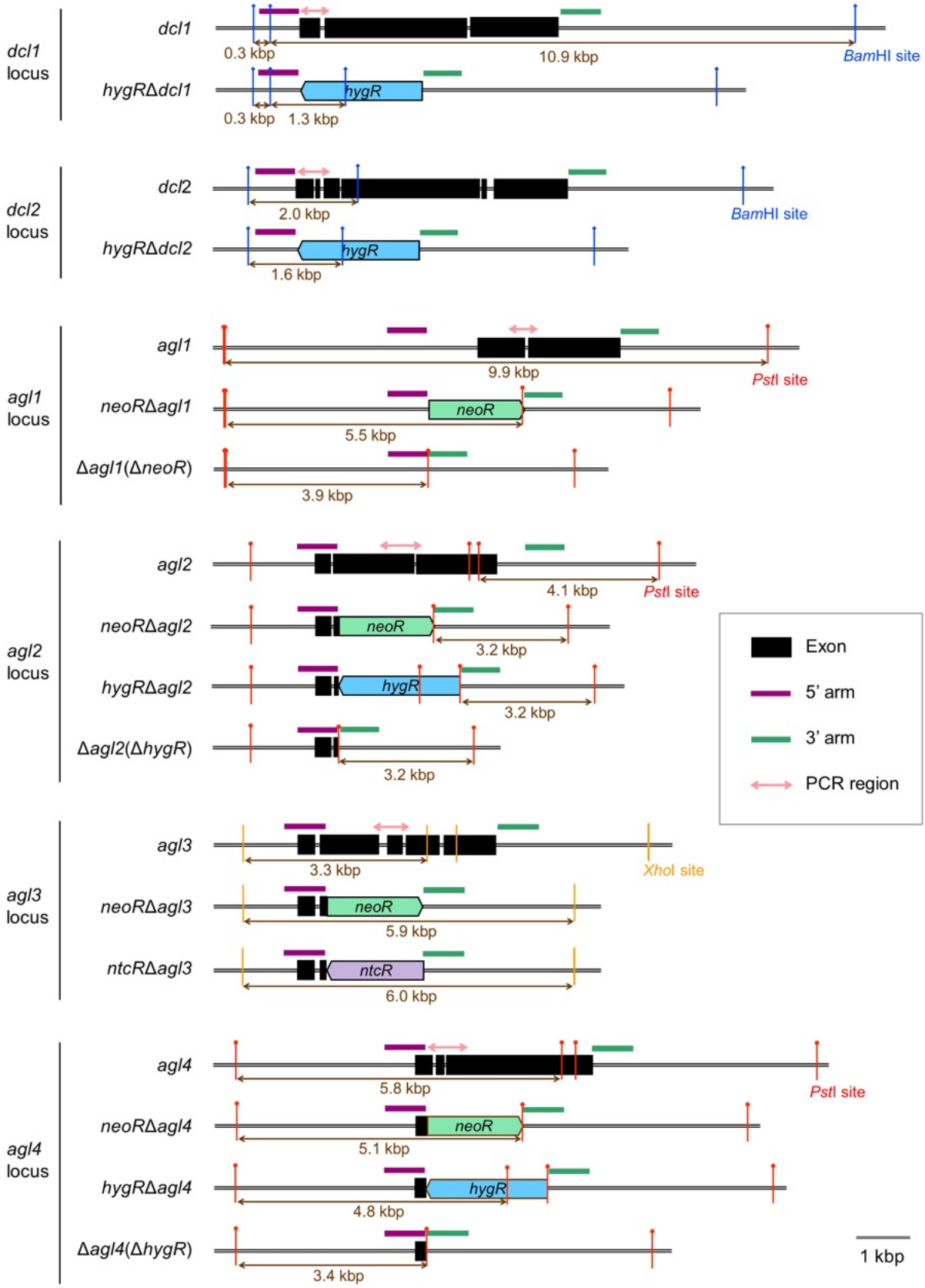

Supplementary Fig. S1. Gene organization and restriction map of wild-type and modified *dcl* and *agl* loci in *Cryphonectria parasitica* DK80.

The organization of wild-type genes is based on a genome assembly of *C. parasitica* strain EP155 (isogenic strain to DK80 except for the *cpku80* locus) (24). The v2.0 unmasked nuclear assembly was searched with *dcl1*, *dcl2*, *agl1*, *agl2*, *agl3*, and *agl4* sequences (*SI Appendix*, Table S4) to obtain the flanking upstream and downstream sequences. The genomic regions are represented by the double lines on which DCL/AGL coding parts (exons) are depicted by the black boxes. The pink two-headed arrows show polymerase chain reaction (PCR) genotyping target regions (Fig. 1*B*). The purple and green boxes indicate the position of the 5′ and 3′ homology arms for gene disruption by homologous recombination. *neoR*, *hygR*, and *ntcR* indicate antibiotic resistance (*R*) gene expression cassettes against neomycin, hygromycin, and nourseothricin, respectively. These antibiotic *R* genes were removed from several gene knockout strains by the Cre-*loxP* system (*SI Appendix*, Fig. S2). The map shows the restriction sites used for Southern blotting (*SI Appendix*, Fig. S3) and the expected fragment length of the probe targets.

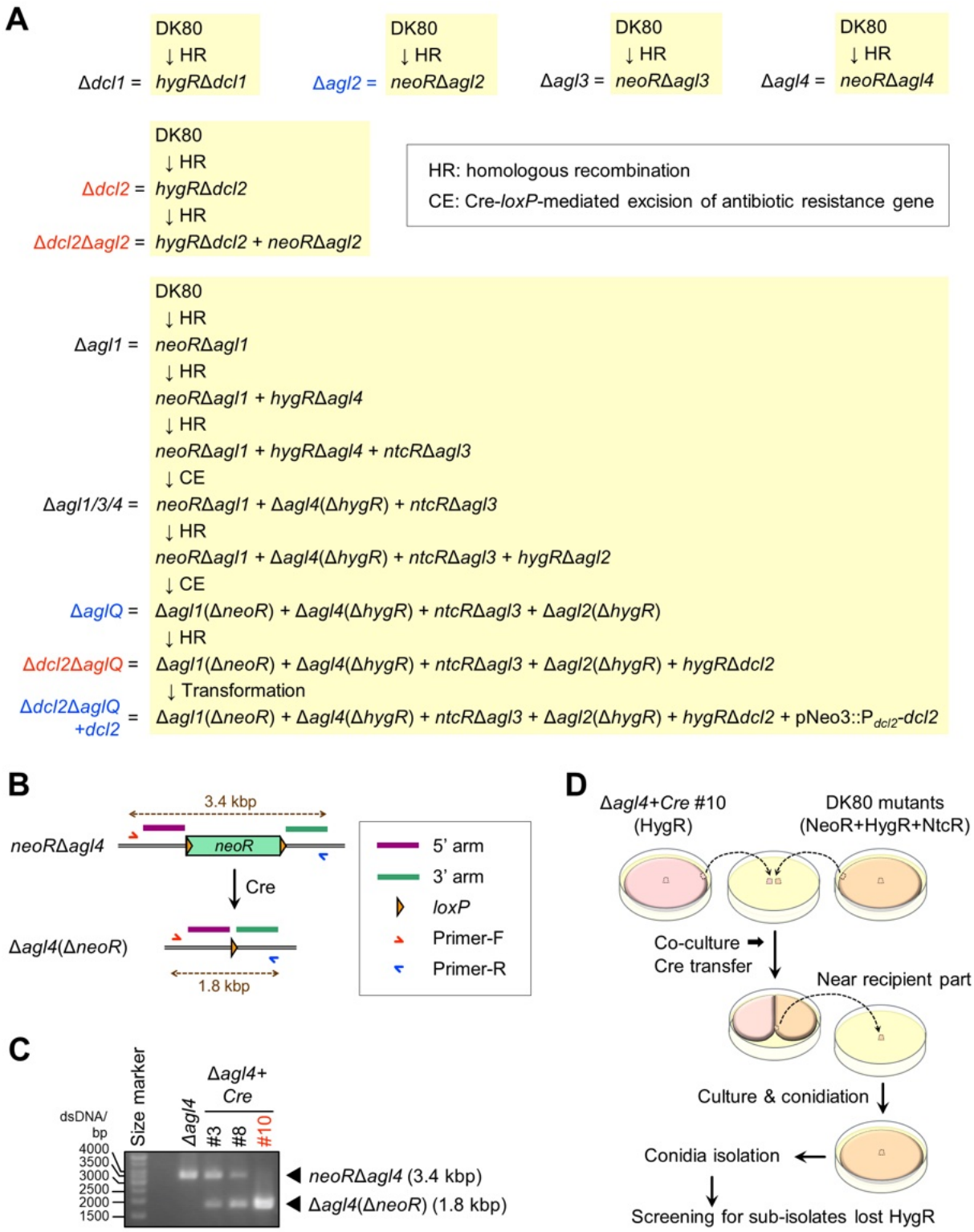

Supplementary Fig. S2. Generation of single and multiple *dcl*/*agl* knockout strains in *Cryphonectria parasitica* DK80. (*A*) Steps to generate the single or multiple *dcl*/*agl* gene knockout strains and a *dcl2* complementary strain. *SI Appendix*, Fig. S1 depicts the structure of the modified genes. **(*B*)** Schematic representation for excision of the antibiotic *R* marker gene by Cre-*loxP* system. An example of Δ*agl4* (*neoR*Δ*agl4*) is shown. Cre recombinase excised the antibiotic *R* gene wedged

between the *loxP* sequences. **(*C*)** Selection of Δ*agl4+Cre* with high Cre efficacy by polymerase chain reaction (PCR). The PCR targets upstream and downstream of the excised region (***B***) (*SI Appendix*, Table S2) to distinguish the presence or absence of *neoR* by amplicon length. Strain #10 showing complete *neoR* excision was selected as a Cre donor. **(*D*)** The strategy for antibiotic *R* gene excision from the *agl* multiple mutants that show multiple resistance to neomycin, hygromycin, and nourseothricin (NeoR, HygR, and NtcR, respectively), by transiently introducing Cre from dual-cultured Δ*agl4+Cre* #10. Refer to the Methods section for the detailed procedure.

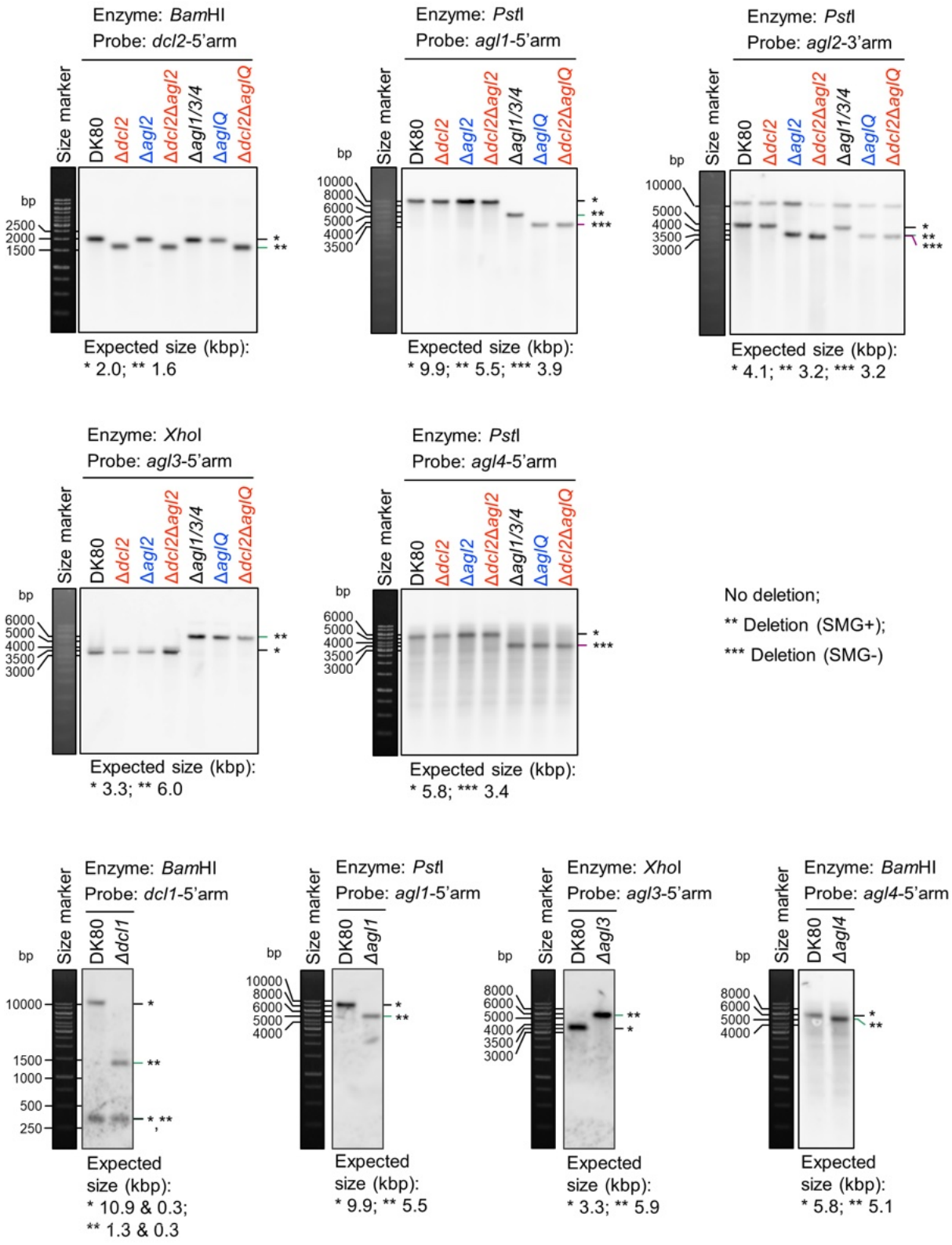

Supplementary Fig. S3. Genotyping of the *dcl*/*agl* knockout strains of *Cryphonectria parasitica* generated in this study. Validation of the targeted genetic modification of Argonaute-like protein genes (*agl1*, *agl2*, *agl3*, and *agl4*) and Dicer-like protein genes (*dcl1* and *dcl2*) by Southern blotting. The probes target the upstream or downstream regions of the deleted regions (*SI Appendix*, Fig. S1). The asterisks indicate the position of the wild haplotype (*), the deletion haplotype carrying the selectable

marker gene (SMG) (**), or another deletion haplotype in which the SMG was removed by the Cre-*loxP* system (***) (*SI Appendix*, Figs. S1 and S2). The Southern hybridization gels were flanked with the size marker stained with ethidium bromide before the blotting.

Supplementary Fig. S4. Colony morphology of the *dcl2/agl* single and multiple knockout strains of *Cryphonectria parasitica*. Virus-free DK80 and its mutants were cultured on potato dextrose agar (9 cm in diameter) for 6 days after a small (1 mm^3) mycelial plug was placed on the center of each plate. The white bar represents 3 cm.

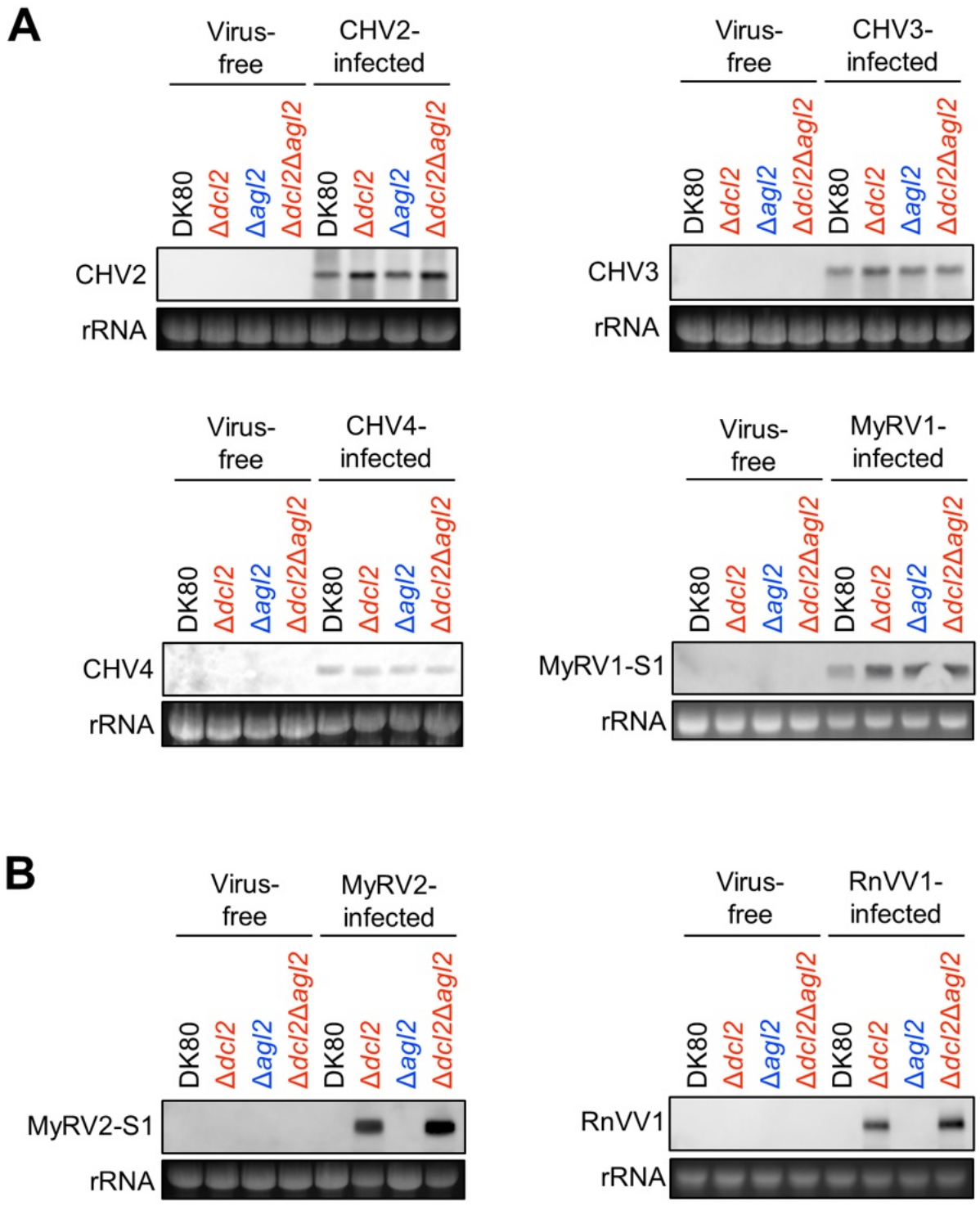

Supplementary Fig. S5. Screening of viruses that are suppressed by *dcl2* but not *agl2*. DK80, Δ*dcl2*, Δ*agl2*, and Δ*dcl2*Δ*agl2* were inoculated with viruses via hyphal fusion (Fig. 2*A*). Viral RNA in the recipients in the absence or presence of the viruses was detected by northern hybridization from crude RNA precipitated with LiCl. Host ribosomal RNA (rRNA) is shown as a loading control. **(*A*)** Viruses less affected by *dcl2* and *agl2*. **(*B*)** Viruses highly affected by *dcl2* but not *agl2*.

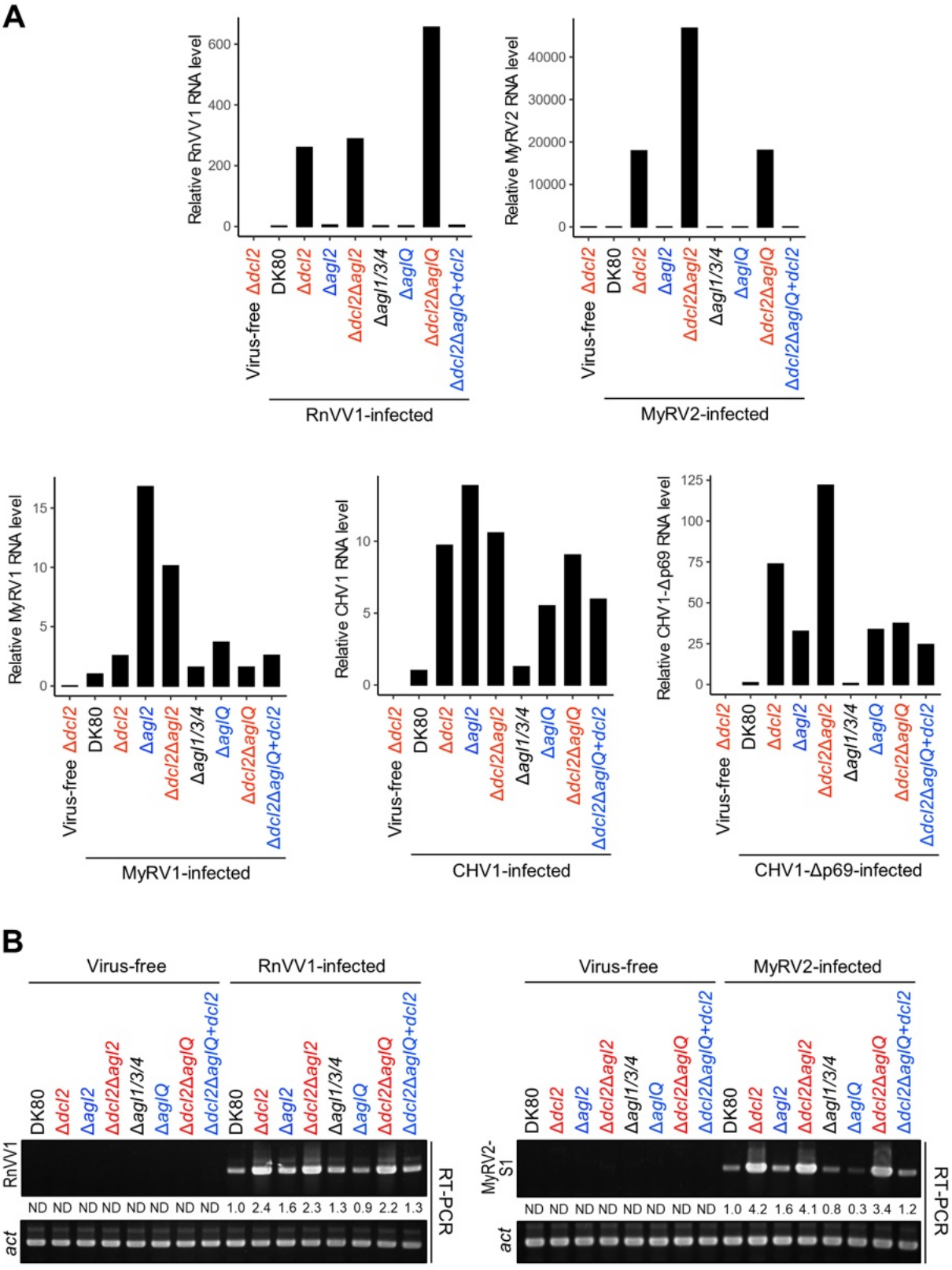

Supplementary Fig. S6. Detection of viral total RNA by quantitative reverse-transcription–polymerase chain reaction (qRT-PCR) and semi-qRT-PCR. The qRT-PCR and semi-qRT-PCR were performed with total RNA (dsRNA + ssRNA) samples used in Fig. 3*A-E*. **(*A*)** qRT-PCR in the fungal

strains inoculated with RnVV1, MyRV2, MyRV1, CHV1, or CHV1-Δp69. The bars indicate fold changes in viral RNA level normalized by the host actin gene expression. The fold changes were calculated based on the value of virus-infected DK80 as 1. **(*B*)** Semi-qRT-PCR in the fungal strains inoculated with RnVV1 or MyRV2. The relative band intensity for semi-qRT-PCR of viral RNA is shown below the electrophoretic image. ND stands for not determined/detected. The host actin gene (*act*) was analyzed as an internal control for semi-qRT-PCR.

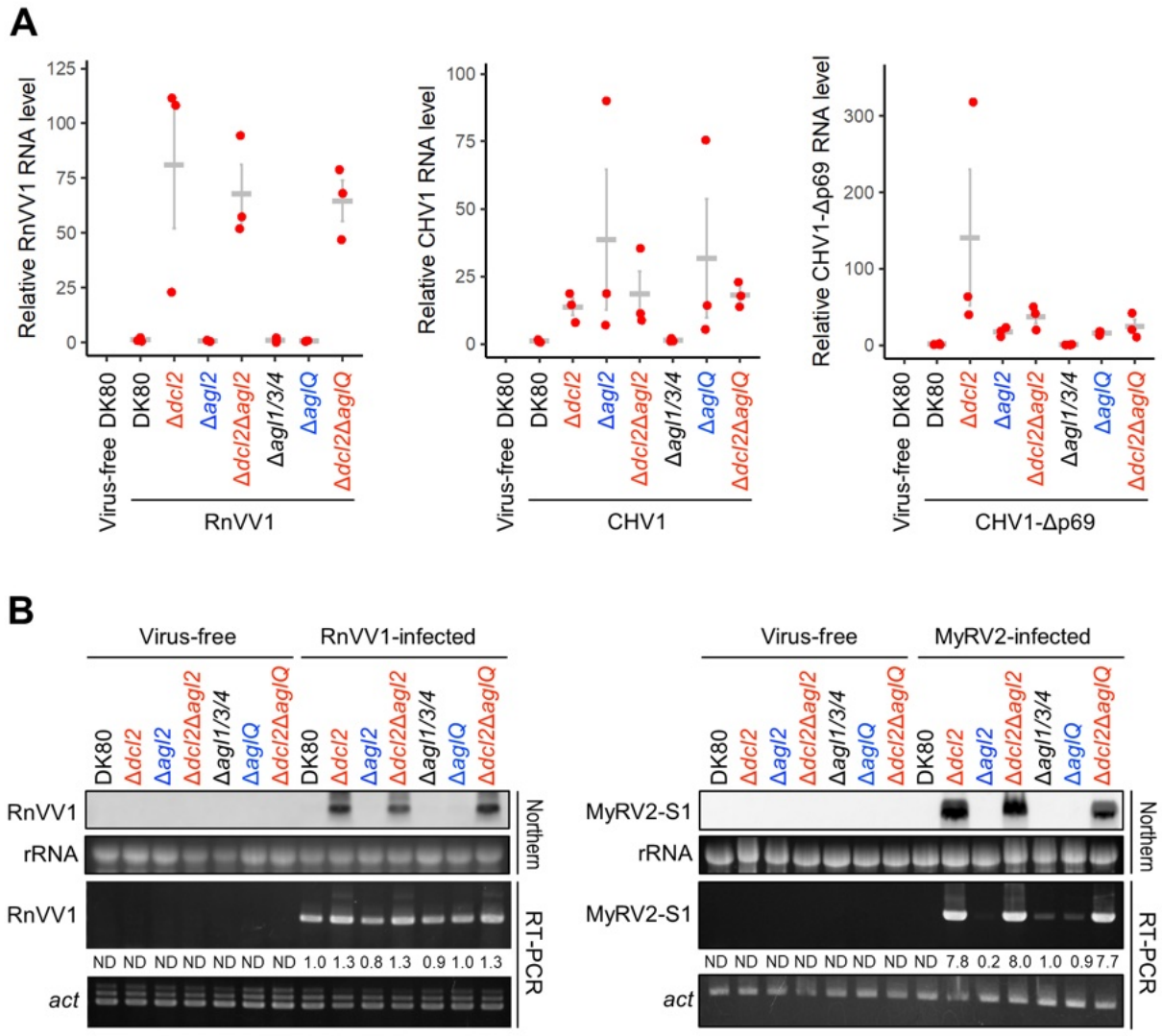

Supplementary Fig. S7. Detection of viral RNA in host ssRNA-enriched nucleic acids by quantitative reverse-transcription–polymerase chain reaction and semi-qRT-PCR. Crude RNA enriched with ssRNA via LiCl was used as a template for cDNA synthesis. **(*A*)** qRT-PCR in the fungal strains inoculated with RnVV1, CHV1, or CHV1-Δp69. The dots indicate fold changes in viral RNA level normalized by the host actin gene expression. The gray cross bars indicate mean values and standard errors in three independent infections. The fold changes were calculated based on the mean value of virus-infected DK80 as 1. **(*B*)** Northern hybridization and semi-qRT-PCR in the fungal strains inoculated with RnVV1 or MyRV2. Host ribosomal RNA (rRNA) is shown as a loading control for northern hybridization. See *SI Appendix*, Fig. S6*B* legend for the details of semi-qRT-PCR.

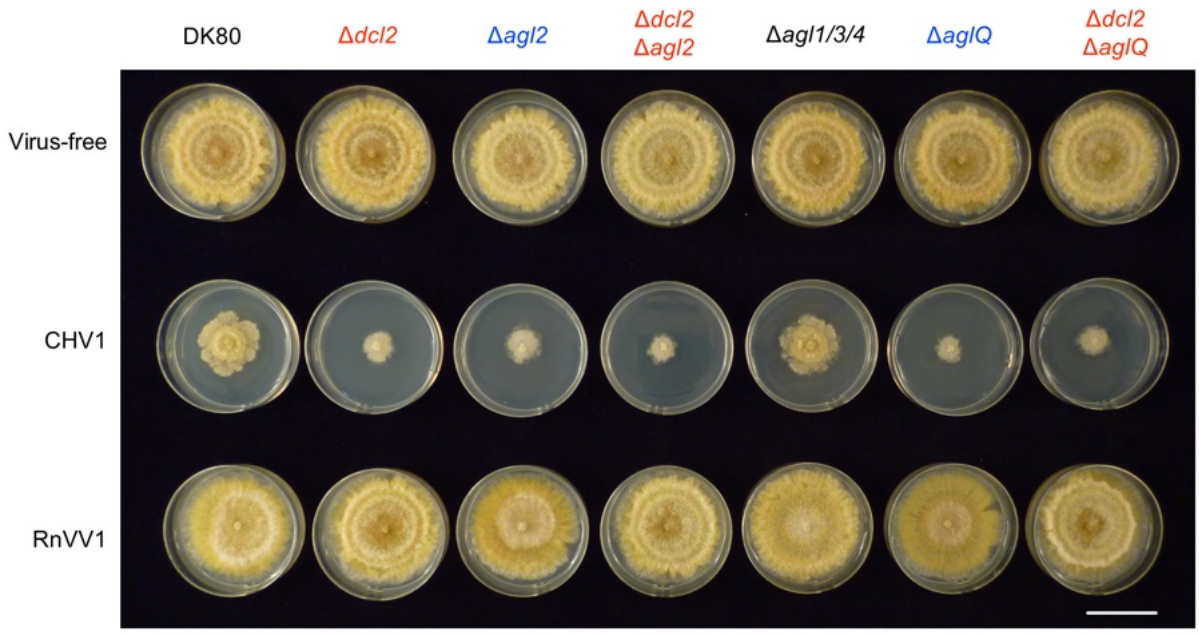

Supplementary Fig. S8. Viral symptoms in the *dcl2/agl* single and multiple knockout strains of *Cryphonectria parasitica*. Another set of fungal colonies infected by CHV1 and RnVV1 was prepared independently from the Fig. 4 experiment. The white bar represents 3 cm.

Supplementary Table S1. Primers used for vector construction

Construct	Target	F/R [a]	Primer sequence (5'-3') [b]
pGEM::loxPneoR	*neoR*	F	GCGGCCGCGGGAATT**ATAACTTCGTATAATGTATGCTATACGAAGTTAT**-gaattcAGATACCCAGAGTTATCTCACCA
		R	AGGCGGCCGCGAATT**ATAACTTCGTATAGCATACATTATACGAAGTTAT**-gaattcTCATTCCCGGTGTAGGAAGC
pGEM::loxPhygRinv	*hygR*	F	ACGAAGTTATGAATTCAGAAGATGATATTGAAGGAGCA
		R	ACGAAGTTATGAATTctagaAAGAAGGATTACCTCTAA
pGEM::loxPntcRinv	*ntcR*	F	ACGAAGTTATGAATTCAGAAGATGATATTGAAGGAGCA
		R	TTAAGTGGATGGATCCTCAGGGGCAGGGCATGCTCA
pGEM::loxPhygRinvΔ*dcl1*	*dcl1*-5'arm	F	ATTGGGCCCGACGTCGCATGCTTCGTCGCTGTTCTGTAATACTG
		R	CCATGGCGGCCGGGAGCATGCCTTGGCCTCGATTTGGGACA
	dcl1-3'arm	F	CGCGGCCGCCTGCAGGTCGACCAGCGATCTGAAGAGTTGTG
		R	GAGCTCTCCCATATGGTCGACCGCGTTGAGATACCCTGTTG
pGEM::loxPhygRinvΔ*dcl2*	*dcl2*-5'arm	F	ATTGGGCCCGACGTCGCATGCACTGACTTTCACAGGTCCAT
		R	CCATGGCGGCCGGGAGCATGCCTTGCAGCGTCGTACGACA
	dcl2-3'arm	F	CGCGGCCGCCTGCAGGTCGACGGTTCGGACCGACAAGAATG
		R	GAGCTCTCCCATATGGTCGACATGAGACACTGATCGTCCTT
pGEM::loxPneoRΔ*agl1*	*agl1*-5'arm	F	ATTGGGCCCGACGTCGCATGCCTCTTCTCTGTGGACCGACCTC
		R	CCATGGCGGCCGGGAGCATGCTGTTGACGACGAGTGCTAGATG
	agl1-3'arm	F	CGCGGCCGCCTGCAGGTCGACAGAGCTCTCTTGTCATGACAGC
		R	CAGCTCTCCCATATGGTCGACCCTGGTCACCATGAGGAACTGC
pGEM::loxPneoRΔ*agl2*, pGEM::loxPhygRinvΔ*agl2*	*agl2*-5'arm	F	ATTGGGCCCGACGTCGCATGCCTTTTCTGCGCATTGCTTTCAT
		R	CCATGGCGGCCGGGAGCATGCAGAACCTAGGCGAGACGCGATA

pGEM::loxPneoRΔ*agl1*, pGEM::loxPntcRinvΔ*agl3*	*agl2*-3'arm	F	CGCGGCCGCCTGCAGGTCGACAACTTTGACGGACCATCCTGTC
		R	GAGCTCTCCCATATGGTCGACTTAGCGTTTGTTGTAGTGTTAA
	agl3-5'arm	F	ATTGGGCCCGACGTCGCATGCTTAATTTCATTTACAAGTAGAC
		R	CCATGGGCGGCCGGGAGCATGCGCCACTAATGCTCAACTGGCTG
	agl3-3'arm	F	CGCGGCCGCCTGCAGGTCGACGGTAGGGAGGGTCGAAAGAAAG
		R	CAGCTCTCCCATATGGTCGACGCTACGCCGCCTCCAAGGCCGG
pGEM::loxPneoRΔ*agl1*, pGEM::loxPhygRinvΔ*agl4*	*agl4*-5'arm	F	ATTGGGCCCGACGTCGCATGCTTTCCAGACTGTAGTTTCATTT
		R	CCATGGCGGCCGGGAGCATGCAGGTCCAGAAGAAGCTCCTGCA
	agl4-3'arm	F	CGCGGCCGCCTGCAGGTCGACGACCACCGGCCAGCGAATGGTG
		R	CAGCTCTCCCATATGGTCGACATGCGTATATACCCTGCTGCCT
pCPXHY3::Cre	Cre CDS	F	CAAGCTTGTTAACGCGGCCGCATGTCCAATTTACTGACCGT
		R	GGAGATCAGGTCAAGCATGCCTAATCGCCATCTTCCAGC
pXYLHY3	P_{xyl}	F	GTTTGGGCCAGAGCTactagtctcgagAAACTTGCCGGATTTACCCT
		R	CCGCGTTAACAAGCTTGGGATTGTAAGGGGACGATG
pXYLNeo3	*neoR*	F	TGCTTGGGCCTAATgaattcAGATACCCAGATACCCAGAG
		R	ACACTATAGAATACtctagaTCATTCCCGGTGTAGGAAGC
pNeo3::P_{dcl2}-*dcl2*	P_{dcl2}-*dcl2*	F	AGCTACTAGTCTCGAGGTTTTGCTCGACGTCGATGC
		R	GGAGATCAGGTCAAgcatgcGGAGTTCGACGTATCCATGT

[a] Primer orientation (F: forward; R: reverse).

[b] Underlined, bold, and lowercase letters indicate attached sequences of linearized vector terminal, *loxP*, and restriction site, respectively.

Supplementary Table S2. Primers used for detection of viruses and host genes

Target gene/virus	Accession:position [a]	F/R* [b]	Primer sequence (5'-3')	Amplicon length (bp) [c]
agl4 flanking regions (*SI Appendix*, Fig. S3*C*)	Crypa2|scaffold_6: 301638-306290	F	CCCATATTCATCTTCTGCACC	*neoR*Δ*agl4*: 3440; Δ*agl4*(Δ*neoR*): 1786
		R	(*agl4*-3'arm reverse) [d]	
dcl1 ORF	DQ186989.1:825-1391	F	ATGGGTGATCCAGCGGCG	gDNA: 567
		R	AAGCCACCTTTTCGACCAGG	
dcl2 ORF	DQ186990.1:1569-2146	F	ATGGCGTACTATACCGACTC	gDNA: 597; cDNA: 424
		R	CGCCTGTGACGATTTTGGTC	
agl1 ORF	GQ250184.1:1011-1521	F	TGCACGGGATCATTCAGAGG	gDNA: 511
		R	CGCTGGCATGCAAATCTAATC	
agl2 ORF	GQ250185.1:1908-2724	F	GTATGGCGTCAATCCCAATG	gDNA: 836; cDNA: 682
		R	CACCTTGCTGCTAGGTTTGG	
agl3 ORF	GQ250186.1:2311-2974	F	CTCGAAGAAGTCACCACCAC	gDNA: 664
		R	ATTGAGAGTTCTGTCCCCGT	
agl4 ORF	GQ250187.1:1196-1951	F	CCTCCTGCTCTCGGATATGA	gDNA: 756
		R	AGTTTCGCTTTATGGCAACCAG	
act ORF (northern, semi-qRT-PCR)	MU032352.1:558771-559410	F	ATGGCGGATTCACTGCACAA	gDNA: 640; cDNA: 520
		R	TGGCAAACCCCTCGTACACC	
act cDNA (qRT-PCR)	XM_040926251.1:622-736	F	GACGTTGAGCGAAGAGCACC	115
		R	GTAGAGAGCGGGGACGTTGA	
CHV1 (northern)	M57938.1:9157-9646	F	TGTACACCTCGTGTGAACGG	490
		R	TGAGTGTGCCACGGATTCTC	
CHV1 and CHV1-Δp69 (qRT-PCR)	M57938.1:9543-9646	F	ATAGTGGACGGGGTGTATCG	104
		R	TGAGTGTGCCACGGATTCTC	

CHV1-Δp69 (northern)	M57938.1:3265-3764	F	TGGAAGAGGCGAAAGAGGCA	500
		R	TGTCGAAGGGTTGGTATTAT	
RnVV1 (northern, semi-qRT-PCR)	AB742454.1:3970-4556	F	TCAACAGTCACCACTCGACG	606
		R	TTGATTTCCCGTGGCGTACA	
RnVV1 (qRT-PCR)	AB742454.1:4441-4575	F	TCAACCCCAACCCGATGACA	135
		R	TTGATTTCCCGTGGCGTACA	
MyRV1-S1 (northern)	AY277888.1:2662-3112	F	AACTTTCGCCCTACGCATGA	451
		R	TGGCGAGAGTTCCATTGCAT	
MyRV1-S1 (qRT-PCR)	AY277888.1:3004-3112	F	CGATTCAAGTGCTACGGCAT	109
		R	TGGCGAGAGTTCCATTGCAT	
MyRV2-S1 (northern)	See legend [e]	F	GGTTTCTCCCCGAGATAGCG	537
		R	AGGTTCTTACAGCTGACCGC	
MyRV2-S1 (qRT-PCR)	See legend [e]	F	GCAATATGCTCACCGTGGTA	135
		R	AGGTTCTTACAGCTGACCGC	
CHV2	L29010.1:3138-3590	F	CATTTCCGAAGAGCCATGCG	453
		R	CCGAATTCCAAGCGCATCAG	
CHV3	AF188515.1:2045-2082	F	AGAGGGTTATGCCCCCTGAT	538
		R	ATCTGCCATCTATCAGCCGC	
CHV4	MK533145.1:287-875	F	ATGTCTGAGCAACAACTCATCT	589
		R	TGCCATCCACCAGATGCCAGTT	

[a] The accession number in JGI Genome Portal is shown for "*agl4* flanking regions", while that in GenBank is listed for the others.

[b] Primer orientation (F: forward; R: reverse).

[c] gDNA: genomic DNA of *C. parasitica*; cDNA: complementary DNA reverse transcribed from messenger RNA of *C. parasitica* or viruses.

[d] Primer sequence is included in *SI Appendix*, Table S1.

[e] Personally provided by Dr. Bradley I. Hillman (Rutgers University).

Supplementary Table S3. Viral and fungal strains used in this study

Strain	Description	Reference
Viral		
CHV2	Capsidless non-segmented (+)RNA virus in the genus *Hypovirus* in the family *Hypoviridae*, from *C. parasitica* strain NB58	(31)
CHV3	Capsidless non-segmented (+)RNA virus in the genus *Hypovirus* in the family *Hypoviridae*, from *C. parasitica* strain GH2	(32)
CHV4	Capsidless non-segmented (+)RNA virus in the genus *Hypovirus* in the family *Hypoviridae*, from *C. parasitica* strain C18	(33)
Fungal		
EP155/CHV2	*C. parasitica* EP155 inoculated with CHV2 isolate NB58	(34)
EP155/CHV3	*C. parasitica* EP155 inoculated with CHV3 isolate GH2	(34)
EP155/CHV4	*C. parasitica* EP155 inoculated with CHV4 isolate C18	This study
Δagl4+Cre	*C. parasitica* DK80*Δagl4* transformed with pCPXHY3::Cre	This study

Supplementary Table S4. ID of RNAi genes in *C. parasitica* EP155/DK80.

Gene name	GenBank accession	Gene ID in Crypa2 [a]	Transcript ID in Crypa2 [a]	Reference
rdr1	HF912382	e_gw1.11.21.1	270014	(35)
rdr2	HF912383	Crypa1.e_gw1.1.1699.1	35624	
rdr3	HF912384	Crypa1.gw1.4.33.1	10929	
rdr4	HF912385	fgenesh1_pm.4_#_888	339656	
dcl1	DQ186989	Crypa1.fgenesh1_pg.C_scaffold_3001033	69967	(36)
dcl2	DQ186990	estExt_Genewise1.C_41219	276559	
agl1	GQ250184	Crypa1.fgenesh1_pg.C_scaffold_9000048	74333	(4)
agl2	GQ250185	estExt_Genewise1Plus.C_60308	292762	
agl3	GQ250186	e_gw1.9.51.1	268359	
agl4	GQ250187	e_gw1.6.1921.1	261854	

[a] *Cryphonectria parasitica* EP155 v2.0 genome assembly (https://mycocosm.jgi.doe.gov/Crypa2) (24).